Cyclophanes and [2]Catenanes as Ligands for Transition Metal Complexes: Synthesis, Structure, Absorption Spectra, and Excited State and Electrochemical Properties**

Peter R. Ashton, Vincenzo Balzani,* Alberto Credi, Oldrich Kocian, Dario Pasini, Luca Prodi, Neil Spencer, J. Fraser Stoddart,* Malcolm S. Tolley, Margherita Venturi, Andrew J. P. White, and David J. Williams*

Abstract: Two novel cyclophanes ($\mathbf{L_1}^{4+}$ and $\mathbf{L_2}^{4+}$), derived from the previously investigated cyclobis(paraquat-*p*-phenylene) tetracation by the replacement of one and two *p*-phenylene spacers by 2,2′-bipyridine units suitable as binding sites for the coordination of transition metals, have been synthesized, as have the [2]catenanes $\mathbf{L_3}^{4+}$ and $\mathbf{L_4}^{4+}$ incorporating $\mathbf{L_1}^{4+}$ and the macrocyclic polyethers bis-*p*-phenylene-34-crown-10 and 1,5-dinaphtho-38-crown-10. $\mathbf{L_1}^{4+}$, $\mathbf{L_2}^{4+}$, $\mathbf{L_3}^{4+}$, and $\mathbf{L_4}^{4+}$ were then used to synthesize some novel mono- and binuclear ruthenium(II), rhenium(I), silver(I), and copper(I) complexes, which were characterized by mass spectrometry, NMR spectroscopy, and, where possible, X-ray crystallography. The absorption spectra, luminescence properties, and electrochemical behavior of the $\mathbf{L_1}^{4+}$, $\mathbf{L_2}^{4+}$, and $\mathbf{L_4}^{4+}$ ligands and the complexes $[Re(CO)_3\mathbf{L_1}Cl]^{4+}$, $[Re(CO)_3\mathbf{L_4}Cl]^{4+}$, $[\{Re(CO)_3Cl\}_2\mathbf{L_2}]^{4+}$, $[Ru(bpy)_2\mathbf{L_1}]^{6+}$, $[Ru(bpy)_2\mathbf{L_4}]^{6+}$, and $[\{Ru(bpy)_2\}_2\mathbf{L_2}]^{8+}$ were investigated. Besides the ligand-centered bands, the Re^{I} and Ru^{II} complexes display metal-to-ligand charge-transfer (MLCT) bands in the visible region similar to those of model compounds $[Re(CO)_3(Cl)(bpy)]$ and $[Ru(bpy)_3]^{2+}$. None of the complexes studied emits at room temperature, because the potentially luminescent MLCT excited state undergoes electron-transfer quenching by the paraquat-type units in the ligands. In a rigid matrix at 77 K, where electron transfer cannot occur, emission is observed from the complexes containing the cyclophane ligands $\mathbf{L_1}^{4+}$ and $\mathbf{L_2}^{4+}$, but not from those containing the catenane ligand $\mathbf{L_4}^{4+}$, in which quenching can still take place by energy transfer to a low-energy CT excited state of the catenane moiety. In the potential window examined (−2.2/+2.1 V), $\mathbf{L_1}^{4+}$ and $\mathbf{L_2}^{4+}$ can accept reversibly five and six electrons, respectively, with processes localized on their paraquat- or bpy-type units. The catenane ligand $\mathbf{L_4}^{4+}$, besides the reduction processes associated with the $\mathbf{L_1}^{4+}$ cyclophane, undergoes two oxidation processes involving the dioxynaphthalene moieties of the crown ether. The complexes exhibit several redox processes (up to a total of nine exchanged electrons in the case of $[Ru(bpy)_2\mathbf{L_4}]^{6+}$ and $[\{Ru(bpy)_2\}_2\mathbf{L_2}]^{8+}$) that can be assigned to i) reduction of the paraquat- and bpy-type moieties of the ligands, ii) reduction of the bpy ligands (in the Ru complexes), iii) oxidation of the metals, and iv) oxidation of the dioxynaphthalene units of the crown ether (in complexes containing the catenane ligand).

Keywords: catenanes · cyclophanes · electrochemistry · luminescence · transition metals

Introduction

Supramolecular chemistry has been considerably enriched by the introduction of abiotic systems capable of self-assembling and self-organizing with a high degree of selectivity.[1] The coordination of transition metals to nitrogen-containing aromatic ligands has been exploited by several research groups as a viable recognition motif for the construction of complex and fascinating molecular architectures, such as double and triple helicates,[2] catenates,[3] molecular knots,[4]

[*] Prof. J. F. Stoddart,[+] Dr. O. Kocian, Dr. D. Pasini, Dr. N. Spencer, P. R. Ashton, M. S. Tolley
School of Chemistry, University of Birmingham
Edgbaston, Birmingham B15 2TT (UK)

Prof. D. J. Williams, Dr. A. J. P. White
Chemical Crystallography Laboratory
Department of Chemistry, Imperial College
South Kensington, London SW7 2AY (UK)
Fax: (+ 44) 171-594-5804

Prof. V. Balzani, A.Credi, L. Prodi, M. Venturi
Università degli Studi di Bologna
Dipartimento di Chimica G. Ciamician
Via Selmi 2, 40126 Bologna (Italy)
Fax: (+ 39) 51-259-456

[+] Current address: Department of Chemistry and Biochemistry
University of California at Los Angeles
405 Hilgard Avenue, Los Angeles, CA 90095-1569 (USA)

[**] Molecular Meccano, Part 35. For Part 34, see P. R. Ashton, M. C. T. Fyfe, S. K. Hickingbottom, S. Menzer, J. F. Stoddart, A. J. P. White, D. J. Williams, *Chem. Eur. J.*, previous paper in this issue.

0947-6539/98/0404-0590 $ 17.50+.50/0 *Chem. Eur. J.* **1998**, *4*, No. 4

and dendritic systems.[5] Metal–ligand interactions are extremely appealing because of the strength of the coordinative bond and the variety of geometries that one can obtain by changing the central metallic core of transition metal complexes.

Recently, interest has grown rapidly in the design and development of photochemical molecular-level devices capable of performing useful light-induced functions.[6] Transition metal based systems have the advantage over their organic counterparts of significant tunability with respect to the structural and electronic properties of both the inorganic and organic components.[7] Polypyridine transition metal complexes, particularly of Ru^{II}, Re^{I}, and Os^{II}, show great promise as components of photochemical devices.[7–11]

One approach to the construction of interlocked molecular compounds and intertwined supramolecular arrays, based on a self-assembly paradigm, relies upon π-electron-deficient and π-electron-rich subunits of high mutual complementarity. Together with the previously reported [2]catenanes $\mathbf{1}^{4+}$ and $\mathbf{2}^{4+}$,[12] based on the π-electron-deficient cyclobis(paraquat-*p*-phenylene) and the π-electron-rich macrocyclic polyethers bis-*p*-phenylene-34-crown-10 (BPP34C10) and 1,5-dinaphtho-38-crown-10 (1/5DN38C10), we have recently achieved the self-assembly of the [2]catenanes $\mathbf{3}^{4+}$ and $\mathbf{4}^{4+}$ bearing one or two 3,3′-disubstituted bitolyl spacers inserted into the skeleton of the tetracationic cyclophane components.[13]

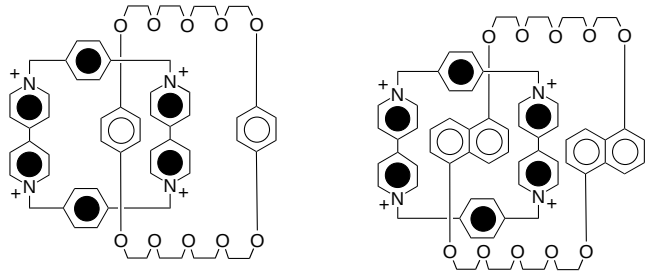

$\mathbf{1}^{4+}$

$\mathbf{2}^{4+}$

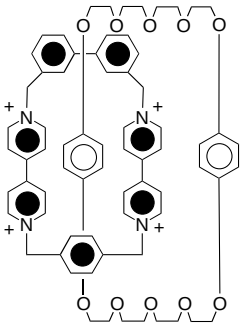

$\mathbf{3}^{4+}$

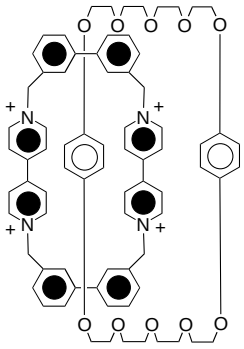

$\mathbf{4}^{4+}$

Herein we describe the syntheses and characterizations of the novel tetracationic cyclophanes $\mathbf{L_1}^{4+}$ and $\mathbf{L_2}^{4+}$ (Scheme 1) and [2]catenanes $\mathbf{L_3}^{4+}$ and $\mathbf{L_4}^{4+}$ (derived from $\mathbf{L_1}^{4+}$ in Scheme 2) containing 2,2′-bipyridine moieties as binding sites for the

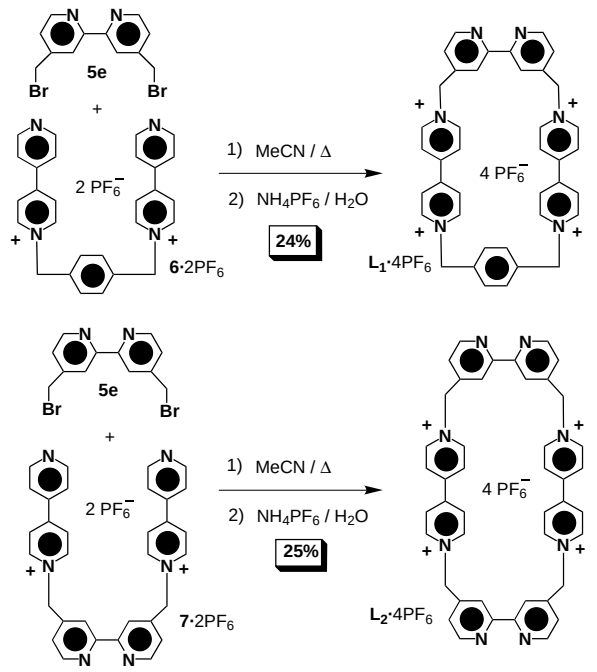

Scheme 1. Synthesis of the tetracationic cyclophanes $\mathbf{L_1}\cdot 4PF_6$ and $\mathbf{L_2}\cdot 4PF_6$, containing one and two 2,2′-bipyridine moieties, respectively.

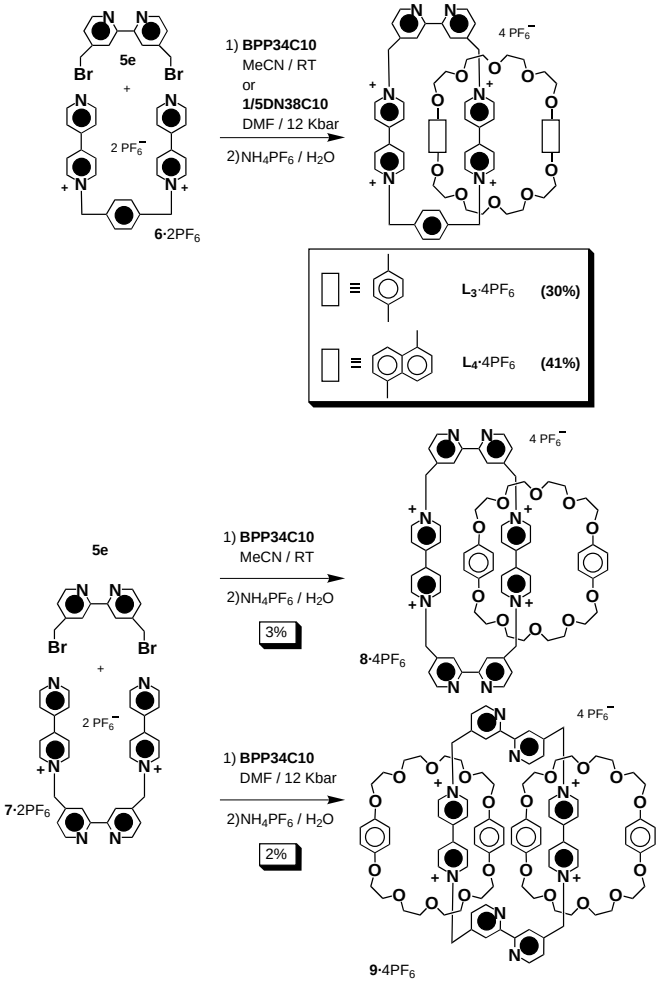

Scheme 2. The self-assembly of the catenanes $\mathbf{L_3}\cdot 4PF_6$, $\mathbf{L_4}\cdot 4PF_6$, $\mathbf{8}\cdot 4PF_6$, and $\mathbf{9}\cdot 4PF_6$; the latter two contain $\mathbf{L_2}$ as their tetracationic cyclophane components.

coordination of a variety of transition metals. We also report the syntheses of novel mono- and binuclear ruthenium(II), rhenium(I), silver(I), and copper(I) complexes of these ligands, and an investigation of the absorption spectra, emission spectra, and electrochemical properties of the $\mathbf{L_1}^{4+}$, $\mathbf{L_2}^{4+}$ and $\mathbf{L_4}^{4+}$ ligands and the $[Re(CO)_3\mathbf{L_1}Cl]^{4+}$, $[Re(CO)_3\mathbf{L_4}Cl]^{4+}$, $[\{Re(CO)_3Cl\}_2\mathbf{L_2}]^{4+}$, $[Ru(bpy)_2\mathbf{L_1}]^{6+}$, $[Ru(bpy)_2\mathbf{L_4}]^{6+}$, and $[\{Ru(bpy)_2\}_2\mathbf{L_2}]^{8+}$ complexes.[14]

Results and Discussion

Synthesis of ligands: The ligands $\mathbf{L_1}^{4+}$ and $\mathbf{L_2}^{4+}$ (Scheme 1) bear the 2,2′-bipyridine unit as a binding site for metal complexation. This unit was incorporated into $\mathbf{L_1}^{4+}$ and $\mathbf{L_2}^{4+}$ via 4,4′-bis(bromomethyl)-2,2′-bipyridine (**5e**). The synthesis of the dibromide **5e** by radical bromination of 4,4′-dimethyl-2,2′-bipyridine (**5a**) has been reported recently.[15] However, in our hands this reaction gave a mixture of polybrominated compounds that was difficult to purify. In the event, we prepared the dibromide **5e** in four steps in 46% yield overall from the commercially available **5a**. We employed the highly efficient method for oxidation of **5a** to **5b** using chromium(VI) oxide in concentrated H_2SO_4 (92% yield) as already reported in the literature.[16] The diacid **5b** was then converted by treatment with MeOH and H_2SO_4 into its dimethyl ester **5c** (84% yield), which was subsequently reduced (79% yield) to the diol **5d** with $NaBH_4$ in EtOH, once again following a literature procedure.[17] Refluxing the diol **5d** with 48% hydrobromic acid produced the dibromide **5e** in 75% yield. The cyclophane $\mathbf{L_1}^{4+}$ was synthesized (Scheme 1) in 24% yield as its hexafluorophosphate salt directly under high dilution conditions (MeCN, reflux) by reaction of the dibromide **5e** with the known[18] bis(hexafluorophosphate) salt $\mathbf{6}\cdot 2PF_6$, followed by flash column chromatography (SiO_2: MeOH/2M aq. NH_4Cl/MeNO$_2$, 7:2:1) and anion exchange (NH_4PF_6/H_2O). The cyclophane $\mathbf{L_2}^{4+}$ was prepared in two steps. Reaction of 4,4′-bipyridine with the dibromide **5e** yielded, after anion exchange (NH_4PF_6/H_2O), the bis(hexafluorophosphate) salt $\mathbf{7}\cdot 2PF_6$ (90% yield), which was cyclized (again under high dilution conditions) with the dibromide **5e** to give (Scheme 1), after flash column chromatography and counterion exchange (NH_4PF_6/H_2O), the tetracationic cyclophane $\mathbf{L_2}^{4+}$ as its hexafluorophosphate salt in 25% yield.

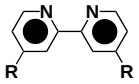

	R
5a	Me
5b	CO_2H
5c	CO_2Me
5d	CH_2OH
5e	CH_2Br

The [2]catenane ligands $\mathbf{L_3}^{4+}$ and $\mathbf{L_4}^{4+}$, containing the macrocyclic polyethers BPP34C10 and 1/5DN38C10, could be prepared at room temperature and at either ambient or ultrahigh pressure using MeCN and DMF as solvents, respectively (Scheme 2). In both cases, one of the precursors of the interlocked rings, either the macrocyclic polyether BPP34C10 or the bis(hexafluorophosphate) salt $\mathbf{6}\cdot 2PF_6$ and the dibromide **5e**, was used in excess. Following chromatography and counterion exchange, $\mathbf{L_3}^{4+}$ and $\mathbf{L_4}^{4+}$ were isolated as their hexafluorophosphate salts in 30 and 41% yields, respectively.

Attempts to incorporate two bipyridine moieties as ligands into the tetracationic cyclophane component of a catenated structure were also made. However, with the crown ether BPP34C10, the yield from the attempted catenation at room temperature and ambient pressure was extremely low: the [2]catenane $\mathbf{8}\cdot 4PF_6$ was isolated in only 3% yield (Scheme 2). Unexpectedly, when the reaction was carried out under ultrahigh-pressure conditions, no [2]catenane was obtained and only a trace of the corresponding [3]catenane $\mathbf{9}\cdot 4PF_6$ was isolated and characterized by mass spectrometry. This result may be explained by the fact that 4,4′-disubstituted-2,2′-bipyridine moieties exist in many different conformations as a consequence of torsion around the aryl–aryl bond. It is believed[18] that, when the tricationic complex is formed (Figure 1), the ring closure to afford the interlocked compound is assisted by effective π–π stacking interactions throughout the system. The preference of 2,2′-bipyridine to exist in an *anti* conformation presumably keeps the bipyridinium and the pyridylpyridinium units of the tricationic intermediate complex too far away from each other for efficient ring closure.[19]

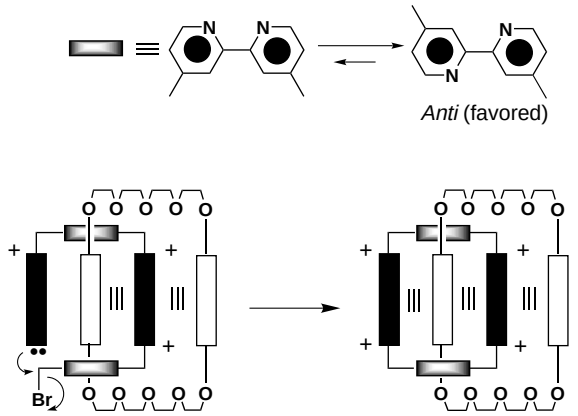

Figure 1. Schematic illustration of a possible route for the formation of the catenanes $\mathbf{8}\cdot 4PF_6$ and $\mathbf{9}\cdot 4PF_6$.

Preparation of Ru^{II} complexes: The ligands $\mathbf{L_1}^{4+}$–$\mathbf{L_4}^{4+}$ were introduced into the bis-heteroleptic mononuclear $[Ru(bpy)_2\mathbf{L_1}](PF_6)_6$, $[Ru(bpy)_2\mathbf{L_3}](PF_6)_6$, and $[Ru(bpy)_2\mathbf{L_4}](PF_6)_6$, and dinuclear $[\{Ru(bpy)_2\}_2\mathbf{L_2}](PF_6)_8$ complexes in 82–97% yields (Schemes 3–5) by reactions of excesses of $\mathbf{L_1}^{4+}$–$\mathbf{L_4}^{4+}$ with $[Ru(bpy)_2Cl_2]$ in EtOH/H_2O.

The Ru^{II} complexes were separated from excesses of the starting materials by treatment of the crude products with H_2O and filtration; after counterion exchange (NH_4PF_6/H_2O), they were purified by slow crystallization/precipitation from iPr$_2$O/MeCN.

Preparation of Re^{I} complexes: The mononuclear $[Re(CO)_3\mathbf{L_1}Cl](PF_6)_4$ and $[Re(CO)_3\mathbf{L_4}Cl](PF_6)_4$ and the dinuclear $[\{Re(CO)_3Cl\}_2\mathbf{L_2}](PF_6)_4$ rhenium(I) tricarbonyl complexes (Schemes 3–5) were obtained in each case by refluxing the ligand ($\mathbf{L_1}^{4+}$, $\mathbf{L_4}^{4+}$, or $\mathbf{L_2}^{4+}$) with an excess of $[Re(CO)_5Cl]$ in anhydrous MeOH. After cooling, the products were collected by filtration and the excesses of the starting materials were

0947-6539/98/0404-0592 $ 17.50+.50/0 *Chem. Eur. J.* **1998**, *4*, No. 4

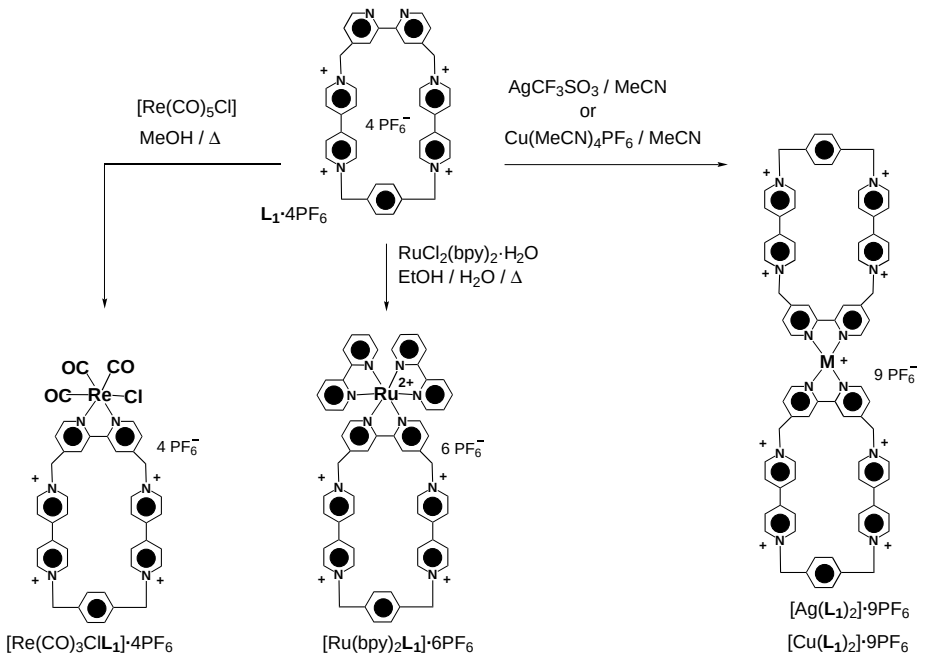

Scheme 3. Preparation of the mononuclear Ag^{I}, Cu^{I}, Re^{I}, and Ru^{II} complexes containing the cyclophane $\mathbf{L}_1^{4+}$.

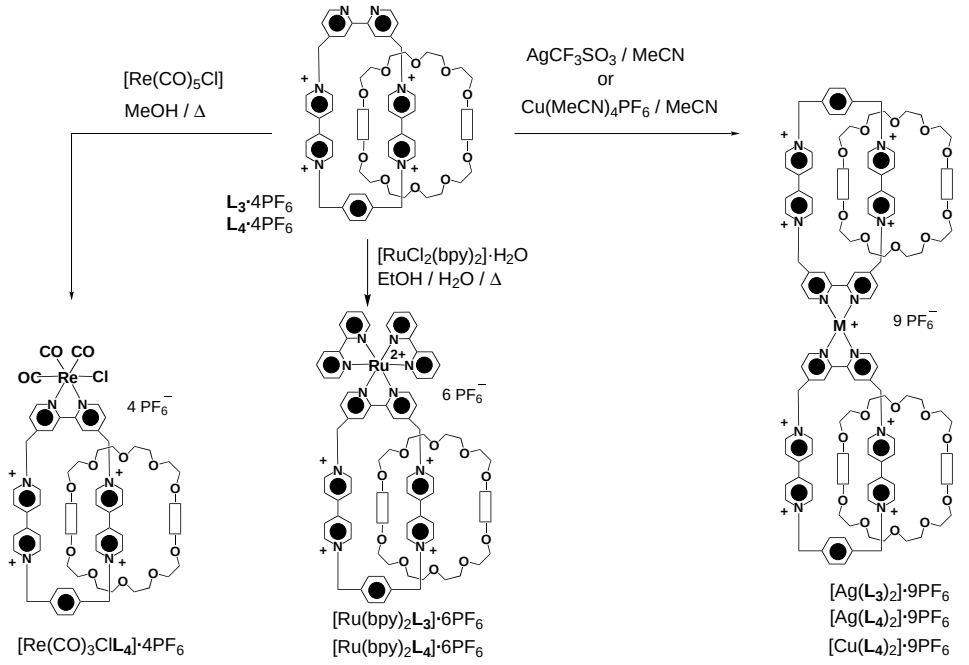

Scheme 4. Preparation of the mononuclear Ag^{I}, Cu^{I}, Re^{I}, and Ru^{II} complexes containing the [2]catenanes $\mathbf{L}_3^{4+}$ and $\mathbf{L}_4^{4+}$.

removed by washing with THF to give the corresponding complexes in 66–82% yield.

Preparation of Ag^{I} and Cu^{I} complexes: The addition of $Ag(CF_3SO_3)$ to MeCN solutions of $\mathbf{L}_1^{4+}$, $\mathbf{L}_3^{4+}$, and $\mathbf{L}_4^{4+}$ in separate experiments led to the isolation of the silver(I) complexes $[Ag(\mathbf{L_1})_2](PF_6)_9$, $[Ag(\mathbf{L_3})_2](PF_6)_9$, and $[Ag(\mathbf{L_4})_2](PF_6)_9$ in 82–93% yields. Similarly, when the ligands $\mathbf{L}_1^{4+}$ and $\mathbf{L}_4^{4+}$ were treated with $[Cu(MeCN)_4](PF_6)$, the complexes $[Cu(\mathbf{L_1})_2](PF_6)_9$ and $[Cu(\mathbf{L_4})_2](PF_6)_9$ were obtained in 83 and 95% yields, respectively (Schemes 3 and 4).

Mass spectrometry of ligands: Liquid secondary ion mass spectrometry (LSIMS) was employed in the characterization of the ligands $\mathbf{L}_1^{4+}$–$\mathbf{L}_4^{4+}$ (Table 1). In all cases, peaks for the successive losses of one, two, or three PF_6^- counterions from the molecular ion were observed. Additionally, the cleavage of the crown ethers from the [2]catenanes $\mathbf{L_3}\cdot 4PF_6$ and $\mathbf{L_4}\cdot 4PF_6$ produces peaks which correspond to the free cyclophane component $\mathbf{L_1}\cdot 4PF_6$, once again with the successive loss of counterions.

In the case of the [3]catenane $\mathbf{9}\cdot 4PF_6$, peaks corresponding to $[M]^+$, $[M-PF_6]^+$, $[M-2PF_6]^+$, and $[M-3PF_6]^+$ at $m/z =$ 2330, 2185, 2040, and 1894 were observed. The loss of one crown ether to produce the corresponding [2]catenane is responsible for peaks at $m/z = 1647$, 1502, and 1357, while loss of the second crown ether produces peaks at $m/z = 1111$, 966, and 821, which correspond to the free cyclophane $\mathbf{L_2}\cdot 4PF_6$ with successive loss of the counterions as usual.

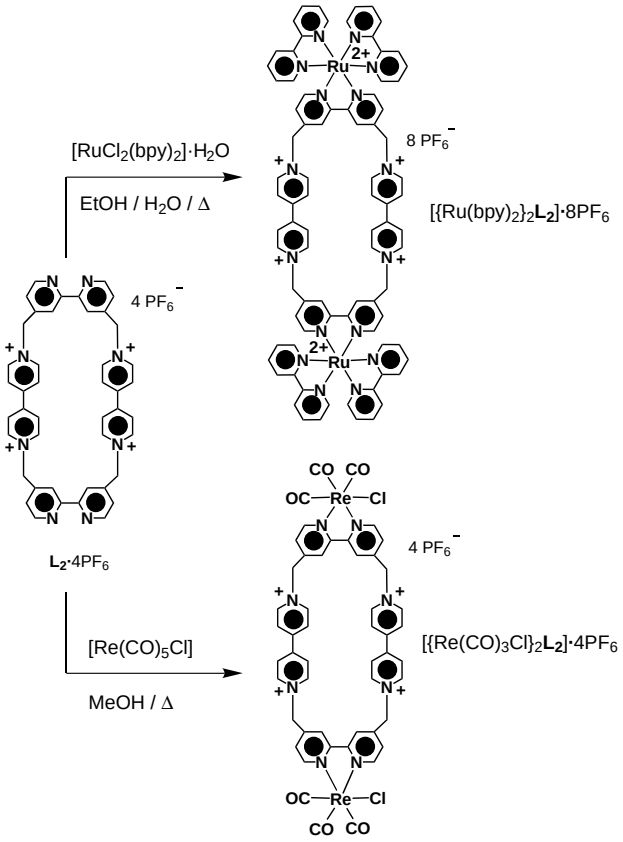

Scheme 5. Preparation of the binuclear Re^{I} and Ru^{II} complexes containing the cyclophane $\mathbf{L}_2^{4+}$.

Table 1. LSIMS data[a] for the bis(hexafluorophosphate) salt $\mathbf{7}\cdot 2PF_6$, the [2]catenane $\mathbf{8}\cdot 4PF_6$, the [3]catenane $\mathbf{9}\cdot 4PF_6$, the ligands $\mathbf{L_1}\cdot 4PF_6$, $\mathbf{L_2}\cdot 4PF_6$, and their corresponding Ru^{II}, Re^{I}, Ag^{I}, and Cu^{I} complexes.

	M[b]	$M-PF_6$	$M-2PF_6$	$M-3PF_6$
$\mathbf{7}\cdot 2PF_6$	(784)[c]	639	493	
$\mathbf{8}\cdot 4PF_6$	(1792)	1647	1502	1357
$\mathbf{9}\cdot 4PF_6$	2330	2185	2040	1894
$\mathbf{L_1}\cdot 4PF_6$	(1178)	1033	888	743
$\mathbf{L_2}\cdot 4PF_6$	(1256)	1111	966	821
$\mathbf{L_3}\cdot 4PF_6$	(1715)	1570	1422	
$\mathbf{L_4}\cdot 4PF_6$	1814	1669	1524	1379
$[Ru(bpy)_2\mathbf{L_1}](PF_6)_4$	(1882)	1737	1592	1447
$[\{Ru(bpy)_2\}_2\mathbf{L_2}](PF_6)_4$	(2664)	2519	2375	2229
$[Ru(bpy)_2\mathbf{L_3}](PF_6)_4$	(2318)	2273	2128	1983
$[Ru(bpy)_2\mathbf{L_4}](PF_6)_4$	(2518)	2373	2229	2084
$[Re(CO)_3Cl\mathbf{L_1}](PF_6)_4$	(1484)	1339	1194	1049
$[Re(CO)_3Cl\mathbf{L_1}](Cl_4)$	(1046)	1011	974	939
$[\{Re(CO)_3Cl\}_2\mathbf{L_2}](PF_6)_4$	(1868)	1723	1578	1433
$[Re(CO)_3Cl\mathbf{L_4}](PF_6)_4$	2120	1975	1830	1685
$[Ag(\mathbf{L_1})_2](PF_6)_9$[d, e]	(2610)	2465	2320	2176
$[Ag(\mathbf{L_3})_2](PF_6)_9$	(3828)	(3683)	3538	3393
$[Ag(\mathbf{L_4})_2](PF_6)_9$[d, f]	(3883)	(3738)	(3593)	(3448)
$[Cu(\mathbf{L_1})_2](PF_6)_9$	(2566)	2420	2274	2130
$[Cu(\mathbf{L_4})_2](PF_6)_9$	(3839)	3693	3549	3403

[a] LSIMS mass spectra were obtained with a VG ZabSpec mass spectrometer equipped with a Cs ion source. [b] M = molecular weight. [c] The numbers in parentheses refer to peaks that were not observed. [d] The spectra were run in a mixture of *m*-nitrobenzylalcohol and DMSO. [e] The fragmentation pattern corresponding to $[M-Ag-2PF_6]^+$, $[M-Ag-3PF_6]^+$, $[M-Ag-4PF_6]^+$ was also observed. [f] The fragmentation pattern corresponding to $[M-Ag-2PF_6]^+$, $[M-Ag-3PF_6]^+$, $[M-Ag-4PF_6]^+$, $[M-Ag-5PF_6]^+$ was observed.

Mass spectrometry of complexes: The results obtained using LSIMS are summarized in Table 1. A general pattern is observed where successive losses of counterions from the molecular ion produce the major significant peaks in the spectra. In the cases of $Ag(\mathbf{L_1})_2\cdot 9PF_6$ and $Ag(\mathbf{L_4})_2\cdot 9PF_6$, it was necessary to predissolve the complexes in DMSO before addition to the *m*-nitrobenzyl alcohol matrix in order to produce satisfactory spectra: ions corresponding to the loss of silver from the molecular ion, in addition to the successive losses of counterions, were detected.

^{1}H NMR spectroscopy of ligands: In the ^{1}H NMR spectra, α-CH, β-CH and α'-CH, β'-CH are used to denote the protons on the 4,4′-bipyridinium units contained between *p*-xylyl and 2,2′-bipyridyl spacers. The convention adopted is one in which α- and β-CH describes the pyridinium ring of the 4,4′-bipyridinium unit which is adjacent to the *p*-xylyl spacer. Thus α'- and β'-CH protons belong to the pyridinium ring which is adjacent to the 2,2′-bipyridyl spacer. The protons on the 2,2′-bipyridyl spacers and on the 2,2′-bipyridine ligands coordinated to ruthenium are marked in the Experimental Section as PyH and bpyH protons, respectively. NOE difference spectroscopy has been used to obtain full proton assignments. In the case of $\mathbf{L_1}^{4+}$ (CD_3CN, 25 °C), irradiation of the methylene protons next to *p*-xylyl spacer at $\delta = 5.77$ leads to an NOE enhancement in the signals for the xylyl protons and α-CH protons at $\delta = 7.56$ and 8.86, respectively. Similarly, irradiation of the NCH_2 protons close to 2,2′-bipyridyl at $\delta = 5.87$ produces an increase in the intensity of the signals for the protons H-5 and H-3 on bipyridyl spacer and the α'-CH protons on the bipyridinium unit at $\delta = 7.88$, 8.13, and 8.92, respectively. Finally, irradiation of α-CH protons yields an enhanced intensity of the β-CH proton signals at $\delta = 8.18$.

The ^{1}H NMR spectra of the [2]catenanes $\mathbf{L_3}^{4+}$ and $\mathbf{L_4}^{4+}$ both showed temperature-dependent behavior. Two dynamic processes (Scheme 6) occurring within these [2]catenanes could be

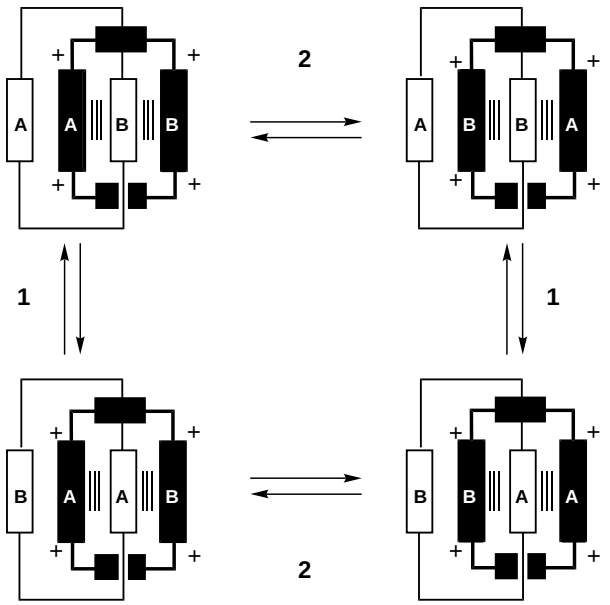

Scheme 6. The dynamic processes occurring in the [2]catenanes $\mathbf{L_3}^{4+}$ and $\mathbf{L_4}^{4+}$ on the ^{1}H NMR time scale.

0947-6539/98/0404-0594 $ 17.50+.50/0 *Chem. Eur. J.* **1998**, *4*, No. 4

identified and characterized. ^{1}H NMR spectra (Figure 2) recorded for the [2]catenane $\mathbf{L}_4^{4+}$ in CD_3CN at 354 K indicate fast circumrotation of the crown ether ring through the tetracationic cyclophane. As a result of this process, two signals each for chemically nonequivalent α-bipyridinium protons, β-bipyridinium protons, and NCH_2 protons are revealed. On cooling a CD_3COCD_3 solution to 243 K, two sets of four signals corresponding to α-bipyridinium protons and β-bipyridinium protons are observed. This temperature-dependent behavior indicates that the circumrotation of the macrocyclic polyether is slow on the ^{1}H NMR time scale and that C_2 symmetry is imposed on the tetracationic cyclophane by the 1,5-dioxynaphthalene residue. When a CD_3COCD_3 solution of the [2]catenane $\mathbf{L}_4^{4+}$ is cooled to 178 K, the circumrotation of the tetracationic cyclophane through the crown ether is slow on the ^{1}H NMR time scale and the two bipyridinium units become anisochronous, since one bipyridinium unit lies inside and the other alongside the cavity of the crown ether. This temperature-dependent behavior is reflected in two sets of eight signals for the α- and the β-protons of the bipyridinium unit. The α/β pairs were assigned following DQF COSY experiments.

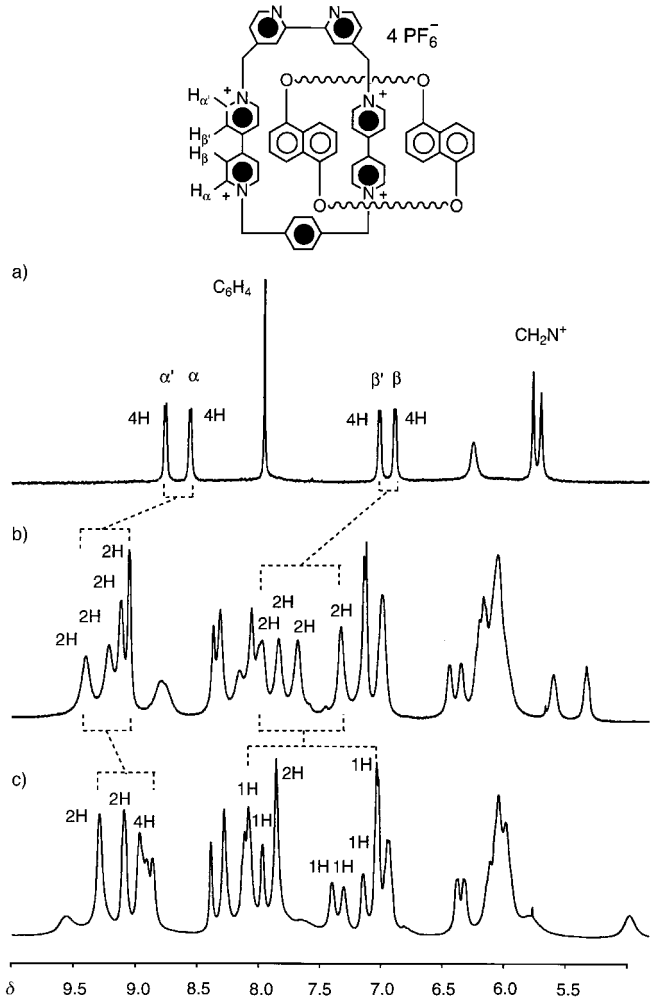

Figure 2. The partial temperature-dependent ^{1}H NMR spectra (400 MHz) of the [2]catenane $\mathbf{L_4}\cdot 4PF_6$ recorded a) in CD_3CN at 354 K, b) in CD_3COCD_3 at 243 K and c) in CD_3COCD_3 at 178 K.

The kinetic and thermodynamic parameters[21] (Table 2) for the circumrotation of the macrocyclic polyether component through the cavity of the tetracationic cyclophane component (process 1 in Scheme 6) show that the activation barrier for this process is decreased upon introduction of one bipyridine spacer into the skeleton of the tetracationic cyclophane component. The activation barriers obtained for the [2]catenanes $\mathbf{L}_3^{4+}$ and $\mathbf{L}_4^{4+}$ are in agreement with the values reported for the [2]catenane $\mathbf{3}^{4+}$ (Table 2), but show a marked decrease when compared with the data obtained for their parent [2]catenanes, $\mathbf{1}^{4+}$ and $\mathbf{2}^{4+}$, with *p*-xylyl spacers present in the tetracationic cyclophane component. This decrease in the activation barrier presumably reflects the reduced stability of the π-acceptor/π-donor/π-acceptor recognition motif in the catenane, as the bipyridinium acceptor units are held further apart, enlarging the cavity of the cyclophane component. The values for the activation energy barriers obtained for process 2 (Scheme 6) in the case of the [2]catenanes $\mathbf{L}_3^{4+}$ and $\mathbf{L}_4^{4+}$, which involves the circumrotation of the tetracationic cyclophane components around the neutral macrocyclic component, do not show any dramatic variation when compared with the [2]catenanes mentioned above (Table 2).

Table 2. Kinetic and thermodynamic parameters[a] for processes 1 and 2 (Scheme 6) obtained from the temperature-dependent 400 MHz ^{1}H NMR spectra of the [2]catenanes $\mathbf{L_3}\cdot 4PF_6$, $\mathbf{L_4}\cdot 4PF_6$, $\mathbf{1}\cdot 4PF_6$, $\mathbf{2}\cdot 4PF_6$, and $\mathbf{3}\cdot 4PF_6$.

[2]catenane	Probe protons	$\Delta\tilde{\nu}$[a] (Hz) ($\Delta\tilde{\nu}$)[b]	k_c[a] (s^{-1}) (k_{ex})[b]	T_c[a] (K) (T_{ex})[b]	$\Delta G_c^{\neq}$[a] (kcal mol^{-1}) ($\Delta G_{ex}^{\neq}$)[b]	Process
$\mathbf{1}\cdot 4PF_6$[c]	OC_6H_4O	(19)	(60)	(313)	(15.7)	1[d]
	α-CH–bpy	74	165	250	12.0	2
$\mathbf{2}\cdot 4PF_6$[e]	$OC_{10}H_6O$	(108)	(240)	(361)	(17.2)	1[f]
	α-CH–bpy	24	75	257	12.7	2
$\mathbf{3}\cdot 4PF_6$[g]	OC_6H_4O	(24)	(75)	(257)	(12.8)	1[f]
	α-CH–bpy	65	144	239	11.5	2
$\mathbf{L_3}\cdot 4PF_6$	OC_6H_4O	714	1586	299	13.1	1[d]
	α-CH–bpy	115	255	229	10.8	2
$\mathbf{L_4}\cdot 4PF_6$	β-CH–bpy	220	489	263	12.1	1[d]
	β-CH–bpy	50	111	189	9.1	2

[a] Data not in parentheses relate to the coalescence method (see ref. [20]). [b] Data in parentheses relate to the exchange method (see ref. [20]). [c] P. R. Ashton, T. T. Godnow, A. E. Kaifer, M. V. Reddington, A. M. Z. Slawin, N. Spencer, J. F. Stoddart, C. Vicent, D. J. Williams, *Angew. Chem.* **1989**, *101*, 1404–1408; *Angew. Chem. Int. Ed. Engl.* **1989**, *28*, 1396–1399. [d] In CD_3COCD_3. [e] P. R. Ashton, C. L. Brown, E. J. T. Chrystal, T. T. Godnow, A. E. Kaifer, K. P. Parry, D. Philp, A. M. Z. Slawin, N. Spencer, J. F. Stoddart, D. J. Williams, *J. Chem. Soc. Chem. Commun.* **1991**, 634–639. [f] In CD_3CN. [g] See ref. [13].

^{1}H NMR spectroscopy of complexes: Selected ^{1}H NMR chemical shift data for the cyclophane ligands $\mathbf{L_1}^{4+}$ and $\mathbf{L_2}^{4+}$, and for the corresponding metal complexes, are listed in Table 3. In the case of the $[Re(CO)_3\mathbf{L_1}Cl]^{4+}$ and $[\{Re(CO)_3Cl\}_2\mathbf{L_2}]^{4+}$ complexes, considerable shifts to the higher frequencies could be observed upon attachment of the electron-withdrawing $Re(CO)_3Cl$ group compared with the same protons in the free ligands $\mathbf{L_1}^{4+}$ and $\mathbf{L_2}^{4+}$. On the other hand, a remarkable shift to lower frequencies has been observed for the H-6 proton resonances of the 2,2′-bipyridyl spacer in all investigated Ru^{II} complexes. The ^{1}H NMR spectra of the Cu^I and Ag^I complexes show no marked differences in chemical shifts upon metal complexation.

In the case of the dinuclear $[\{Ru(bpy)_2\}_2\mathbf{L_2}]^{8+}$ complex, one might expect a mixture of *meso* ($\Lambda\Delta$) and *rac* ($\Lambda\Lambda/\Delta\Delta$) diastereoisomeric forms. Unfortunately, we have not been successful in separation of the diastereoisomeric pairs using base-deactivated reversed phase HPLC with 0.1 % TFA in a H_2O/MeCN solvent gradient.

X-ray crystallography: The X-ray analysis (Figure 3) of $[Re(CO)_3Cl\mathbf{L_1}](PF_6)_4$ shows the tetracationic cyclophane component to have a toboggan-like conformation with the *p*-xylyl and 2,2′-bipyridyl spacers inclined by 92 and 122°, respectively, to the mean plane of the cyclophane (as defined by the four methylene carbon atoms). The 2,2′-bipyridyl portion acts as a bidentate ligand to the Re center, which has distorted octahedral coordination geometry (the angles at Re are in the range 74.4(3) – 99.8(4)° and 172.2(4) – 175.4(3)°, the most acute angle being due to the bite of the 2,2′-bipyridyl ligand). The two Re – N bonds are of the same length (2.167(7), N(1) and 2.165(7), N(8) Å) as are the two *trans* Re – C distances (1.90(1) and 1.91(1) Å). The Re – C bond *trans* to Cl is slightly longer at 1.93(1) Å, reflecting the *trans* effect of the Cl atom; the Re – Cl distance is 2.468(3) Å. There are no significant intercomplex $\pi-\pi$ interactions, though the included benzene solvent molecules enter into both intra- and intercomplex $\pi-\pi$ stacking interactions. One of these interactions involves a benzene molecule inserted into the cyclophane's cavity and sandwiched between the two bipyridinium units (mean interplanar separations of 3.50 and 3.55 Å), an interaction which is supplemented by a $C-H\cdots\pi$ interaction between one of the hydrogen atoms of the benzene molecule and the *p*-xylyl spacer of the cyclophane (the $H\cdots\pi$ distance is 2.88 Å and the associated $C-H\cdots\pi$ angle 178°). The other included benzene molecule is π-stacked between the N(1)-containing pyridyl ring of one complex and its C_i related counterpart of another. The associated ring centroid/ring centroid and interplanar separations are 3.36 and 3.46 Å, respectively.

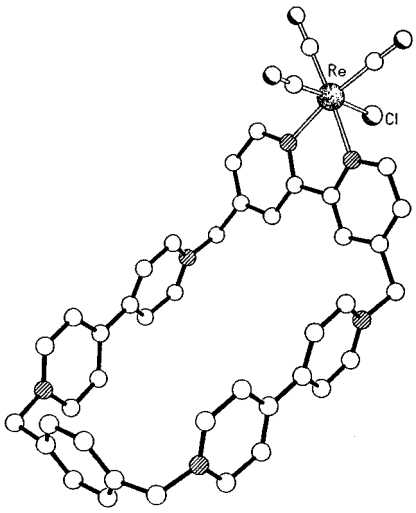

Figure 3. X-ray crystal structure of the complex $[Re(CO)_3\mathbf{L_1}(Cl)](PF_6)_4$.

The X-ray structure (Figure 4) of $[Ag(\mathbf{L_1})_2](PF_6)_9$ shows the 2:1 complex to have crystallographic C_2 symmetry, the geometry at Ag being severely distorted tetrahedral with angles at Ag in the range 71.6(2) – 135.4(2)°. The size of the smaller of these angles is again due to the bite of the 2,2′-bipyridyl ligand, and the other distortion from tetrahedral is due to a twisting of the two $Ag-N_2$ coordination planes about the vector bisecting the N-Ag-N angle by 11° from an

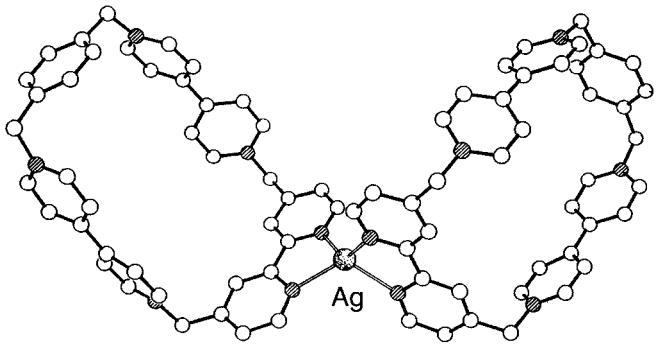

Figure 4. X-ray crystal structure of the complex $[Ag(\mathbf{L_1})_2](PF_6)_9$.

Table 3. ^{1}H NMR chemical shift data [δ values] for ligands and complexes in CD_3CN at ambient temperature.

	Bipyridinium				Py			*p*-Xylyl		
	α′-CH	α-CH	β′-CH	β-CH	H-6	H-3	H-5	CH_2N^+	C_6H_4	CH_2N^+
$\mathbf{L_1}\cdot 4PF_6$	8.92	8.86	8.21	8.18	8.83	8.13	7.88	5.87	7.56	5.77
$[Re(CO)_3Cl\mathbf{L_1}](PF_6)_4$	9.07	8.89	8.21	8.18	9.17	8.51	7.95	5.96	7.64	5.79
$[Ru(bpy)_2\mathbf{L_1}](PF_6)_4$	8.88	8.84	8.16	8.12	7.90	8.33	7.66	5.81	7.63	5.79
$[Ag(\mathbf{L_1})_2](PF_6)_8$	9.00	8.88	8.21	8.19	8.76	8.11	7.73	5.83	7.55	5.75
$[Cu(\mathbf{L_1})_2](PF_6)_4$[a]	9.51	9.44	8.59	8.59	8.77	8.24	7.90	5.91	7.67	5.83
$\mathbf{L_2}\cdot 4PF_6$	8.95	–	8.17	–	8.77	8.27	7.72	5.84	–	–
$[\{Re(CO)_3Cl\}_2\mathbf{L_2}](PF_6)_4$	9.02	–	8.29	–	9.15	8.30	7.93	5.97	–	–
$[\{Ru(bpy)_2\}_2\mathbf{L_2}](PF_6)_8$	8.96	–	8.28	–	7.89	8.30	7.64	5.89	–	–

[a] In CD_3SOCD_3. The δ values for $\mathbf{L_1}\cdot 4PF_6$ in CD_3SOCD_3 are 9.54, 9.44, 8.60, 8.77, 8.24, 7.90, 5.95, 7.68, and 5.83 for the α′-CH, α-CH, β′-CH, β-CH, H-6, H-3, H-5, bpy NCH_2, C_6H_4, and xylyl NCH_2, respectively.

0947-6539/98/0404-0596 $ 17.50+.50/0 *Chem. Eur. J.* **1998**, *4*, No. 4

orthogonal relationship between them. The two independent Ag–N distances are essentially the same at 2.297(5), N(1) and 2.315(5), N(8). The cyclophane has a conformation that is similar to that in the Re complex, although in $[Ag(\mathbf{L_1})_2](PF_6)_9$ the *p*-xylyl and 2,2′-bipyridyl rings are inclined by 84 and 107° to the mean plane of the cyclophane. In common with the Re complex, here again we see the trapping of a benzene solvent molecule within the cyclophane by a combination of a C–H···π interaction to the *p*-xylyl spacer (H···π, 2.65 Å; C–H···π, 160°) and π–π stacking with one of the bipyridinium units (interplanar separation ca. 3.55 Å). The presence of only this single π–π interaction is due to a substantial twist, (ca. 40°) between the two pyridinium rings of one of the bipyridinium units causing an offset of the included benzene ring within the cavity. Inspection of the packing of the 2:1 complex (Figure 5)

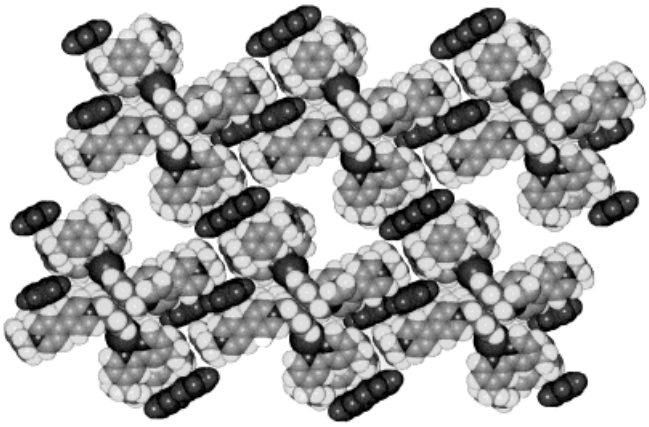

Figure 5. Packing of the molecules of the complex $[Ag(\mathbf{L_1})_2](PF_6)_9$.

reveals an extensive array of both face-to-face and T-type edge-to-face aryl/aryl interactions involving the 2,2′-bipyridyl, a pyridinium, the *p*-xylyl, and the other included benzene solvate molecule (the other benzene molecule is held within the cyclophane; see above). This included benzene molecule is involved in a pair of C–H···π interactions: one of these is to one of the pyridinium rings of the cyclophane (H···π, 2.73 Å; C–H···π, 156°), whereas the other is to the opposite face of the ring from one of the *p*-xylyl hydrogen atoms (H···π, 2.86 Å; C–H···π, 140°). The intercomplex interactions are a parallel π–π stacking between pairs of 2,2′-bipyridyl rings (interplanar separation, 3.41 Å) and a weaker face-to-face interaction (3.77 Å) between the *p*-xylyl ring of one molecule and the pyridinium ring of another, that involved also in a C–H···π interaction with the included benzene molecule.

The X-ray analysis (Figure 6) shows the diruthenium complex $[\{Ru(bpy)_2\}_2\mathbf{L_2}](PF_6)_8$ to have an averaged C_i symmetric geometry.[22] The tetracationic cyclophane, which functions as a bis-bidentate ligand, adopts a chairlike conformation. The two 2,2′-bipyridyl spacers are inclined by 64° to the mean plane of the cyclophane, while the two independent pyridinium rings are tilted steeply inwards, being inclined by 17 and 27° to this plane. The latter two ring-tilts are in opposite senses, thereby producing a 44° twist between them. As a result of these tilts, the macroring is essentially self-filling. The geometry observed at each ruthenium center

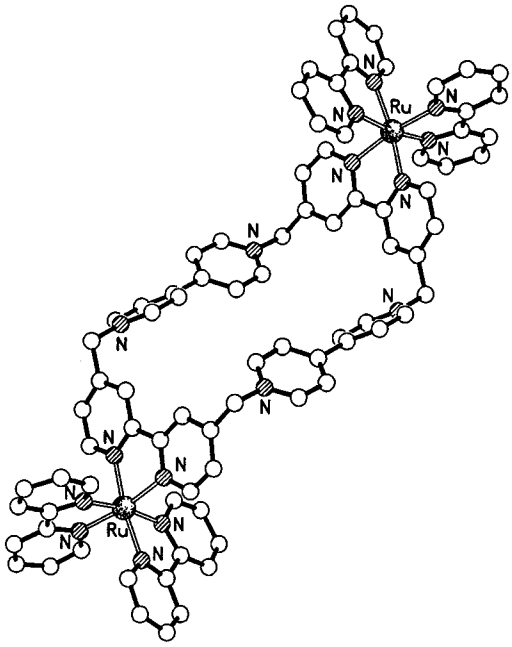

Figure 6. X-ray crystal structure of the complex $[\{Ru(bpy)_2\}_2\mathbf{L_2}](PF_6)_8$.

is disordered, there being a superimposition of Δ and Λ configurations.[23] The crystallographic evidence suggests an inability to produce a resolved (i.e. chiral) complex. What we cannot be certain about is whether we have a structure that is disordered with an equal mixture of ΔΔ and ΛΛ forms or of ΔΛ (and ΛΔ) forms—or, indeed, a mixture of all three diastereoisomers. The shortest intermolecular Ru···Ru separations (9.05 Å) are significantly shorter than the intramolecular separation (17.43 Å) of these atoms.

The X-ray structure (Figure 7) of the [2]catenane $\mathbf{L_4}\cdot 4PF_6$ shows the 2,2′-bipyridyl spacer in the tetracationic cyclophane to have a twisted *anti* conformation (mean twist between the two pyridyl rings of 139°), a geometry distinctly different from that observed in the metal complexes (vide supra). Despite this geometry the four corner methylene carbon atoms are coplanar to within 0.09 Å. The 1/5DN38C10 ring component is threaded in a conventional manner through the center of the tetracationic cyclophane, the inside and alongside $OC_{10}H_6O$ vectors being inclined by 49 and 10°, respectively, to the mean plane of the tetracation. The catenane is stabilized by i) π–π stacking interactions between the inside

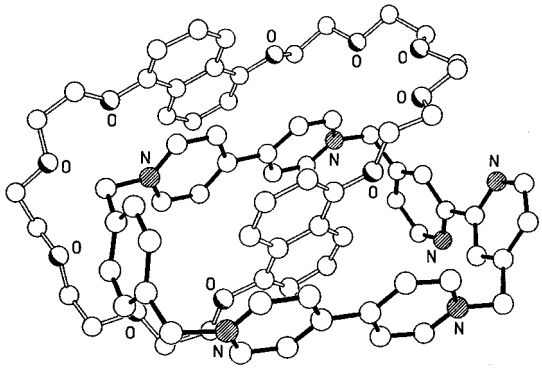

Figure 7. X-ray crystal structure of the [2]catenane $\mathbf{L_4}\cdot 4PF_6$.

1,5-dioxynaphthalene ring system and the inside and alongside bipyridinium units (interplanar separations of 3.45 and 3.59 Å, respectively) and between the alongside 1,5-dioxynaphthalene ring system and the inside bipyridinium unit (interplanar separations of 3.46 Å), and ii) a C–H···π interaction involving one of the *peri* hydrogen atoms on the inside 1,5-dioxynaphthalene ring system and *p*-xylyl ring of the cyclophane (H···π, 2.81 Å; C–H···π, 149°). There are no C–H···O hydrogen bonds. Futhermore, somewhat unusually, there are no extended intermolecular π–π stacking interactions between molecules in the crystal.

Absorption spectra of ligands: The absorption spectra of the ligands $\mathbf{L}_1^{4+}$, $\mathbf{L}_2^{4+}$, and $\mathbf{L}_4^{4+}$ are shown in Figure 8; the wavelengths of the absorption maxima and the molar absorption coefficients are listed in Table 4. The ligands $\mathbf{L}_1^{4+}$ and $\mathbf{L}_2^{4+}$ display strong absorptions in the UV region, consistent with the absorption bands shown by the 2,2′-bipyridyl-[21] and paraquat-type[18] subunits. The catenane ligand $\mathbf{L}_4^{4+}$, besides an intense UV absorption, shows the expected[24] charge-transfer band in the visible region owing to the interaction between the electron-accepting paraquat-type units and the electron-donating dioxynaphthalene units.

Absorption spectra of complexes: The results obtained are summarized in Table 4, where the previously available data for the $[Re(CO)_3(Cl)(bpy)]$ and $[Ru(bpy)_3]^{2+}$ model compounds are also included for comparison purposes. The absorption spectra of the $[Re(CO)_3\mathbf{L_1}Cl]^{4+}$, $[Re(CO)_3\mathbf{L_4}Cl]^{4+}$, and $[\{Re(CO)_3Cl\}_2\mathbf{L_2}]^{4+}$ complexes are shown in Figure 9 and those of the $[Ru(bpy)_2\mathbf{L_1}]^{6+}$, $[Ru(bpy)_2\mathbf{L_4}]^{6+}$, and $[\{Ru(bpy)_2\}_2\mathbf{L_2}]^{8+}$ complexes in Figure 10. The discussion that follows is based on the usual assumption that the ground and excited states of Re^{I} and Ru^{II} polypyridine complexes can be described by localized molecular orbital configurations.[7–11]

The Re^{I} complexes containing a bpy-type ligand are characterized by a metal-to-ligand charge-transfer (MLCT) band at the border between the UV and Vis spectral region resulting from an electron transition from an orbital mainly localized on Re to a π* orbital mainly localized on the bpy-type ligand.[11] In the spectrum of $[Re(CO)_3\mathbf{L_1}Cl]^{4+}$, one can see a strong absorption band below 300 nm, which is due to the paraquat-type and bpy-type chromophoric groups of $\mathbf{L}_1^{4+}$.

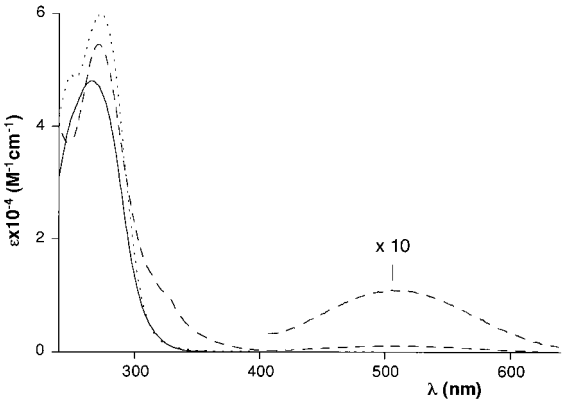

Figure 8. Absorption spectra (MeCN, 298 K) of the ligands $\mathbf{L}_1^{4+}$ (full line), $\mathbf{L}_2^{4+}$ (dotted line), and $\mathbf{L}_4^{4+}$ (dashed line).

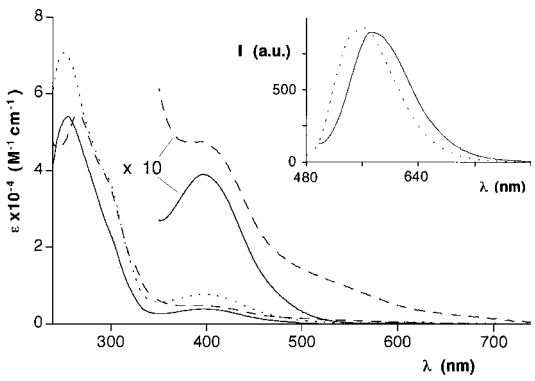

Figure 9. Absorption (MeCN, 298 K) and luminescence (inset: butyronitrile, 77 K) spectra of the complexes $[Re(CO)_3\mathbf{L_1}Cl]^{4+}$ (full line), $[\{Re(CO)_3Cl\}_2\mathbf{L_2}]^{4+}$ (dotted line), and $[Re(CO)_3\mathbf{L_4}Cl]^{4+}$ (dashed line).

Table 4. Absorption and emission properties of ligands and complexes.

	Absorption 298 K[a]		Emission 298 K[a]		Emission 77 K[b]	
	λ_{max} (nm)	ε ($M^{-1}cm^{-1}$)	λ_{max} (nm)	τ (ns)	λ_{max} (nm)	τ (μs)
$\mathbf{L}_1^{4+}$	266	48000	–	–	–	–
$\mathbf{L}_2^{4+}$	273	60000	–	–	–	–
$\mathbf{L}_4^{4+}$	271	55000	–	–	–	–
	512	1100				
$[Re(CO)_3(Cl)(bpy)]$	370[c]	3400[c]	622[c]	25[c]	530[d, e]	3.8[d, e]
$[Re(CO)_3\mathbf{L_1}Cl]^{4+}$	255	54000	–	–	561	3.1
	396	3900				
$[Re(CO)_3\mathbf{L_4}Cl]^{4+}$	394	4800	–	–	–	–
	512	1600				
$[\{Re(CO)_3Cl\}_2\mathbf{L_2}]^{4+}$	250	71000	–	–	579	1.7
	394	7800				
$[Ru(bpy)_3]^{2+}$	450[f]	14300[f]	630[f]	1150[f]	582[f, g]	5.1[f, g]
$[Ru(bpy)_2\mathbf{L_1}]^{6+}$	255	64000	–	–	597	6.0
	285	80000				
	450	11500				
$[Ru(bpy)_2\mathbf{L_4}]^{6+}$	285	80000	–	–	–	–
	470	9000				
$[\{Ru(bpy)_2\}\mathbf{L_2}]^{8+}$	285	132000	–	–	603	5.2
	448	23500				

[a] Acetonitrile solution. [b] Butyronitrile rigid matrix. [c] See ref. [11]. [d] EPA matrix. [e] See ref. [25]. [f] See ref. [7]. [g] In MeOH/EtOH rigid matrix.

0947-6539/98/0404-0598 $ 17.50+.50/0 *Chem. Eur. J.* **1998**, *4*, No. 4

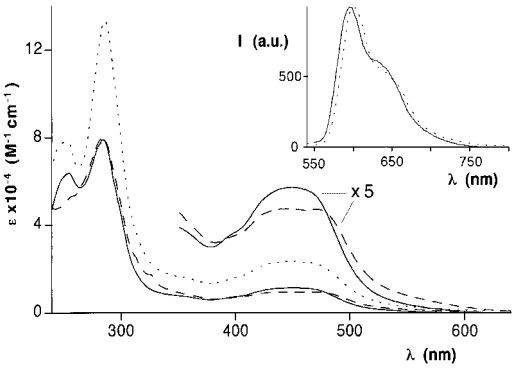

Figure 10. Absorption (MeCN, 298 K) and luminescence (inset: butyronitrile, 77 K) spectra of the complexes $[Ru(bpy)_2\mathbf{L_1}]^{6+}$ (full line), $[\{Ru(bpy)_2\}_2\mathbf{L_2}]^{8+}$ (dotted line), and $[Ru(bpy)_2\mathbf{L_4}]^{6+}$ (dashed line).

The MLCT band is found at considerably lower energy than that in the $[Re(CO)_3(Cl)(bpy)]$ model compound.[11, 25] This difference can be attributed to the Coulombic stabilization offered to the MLCT excited state by the positive charges on the paraquat-type units present in $\mathbf{L}_1^{4+}$. The MLCT band of $[\{Re(CO)_3Cl\}_2\mathbf{L_2}]^{4+}$ occurs at the same wavelength and shows an absorption coefficient twice that of $[Re(CO)_3\mathbf{L_1}Cl]^{4+}$, suggesting that the two metal-based moieties do not substantially perturb each other—a conclusion which is confirmed by the electrochemical results (see below). Comparison of the absorption spectra of $[Re(CO)_3\mathbf{L_1}Cl]^{4+}$ and $[Re(CO)_3\mathbf{L_4}Cl]^{4+}$ indicates that the latter complex displays a more intense absorption in the 300–350 nm spectral region because of the bands due to the 1/5DMN units of the crown ether, and a tail in the 400–600 nm region due to the CT band of the catenane ligand.

It is well known[7, 8] that the Ru^{II} complexes of bpy-type ligands exhibit a MLCT band in the visible region around 450 nm. Besides the ligand-centered bands in the UV region, the absorption spectrum of $[Ru(bpy)_2\mathbf{L_1}]^{6+}$ (Figure 10) shows a MLCT band much broader (toward lower energies) than that of the $[Ru(bpy)_3]^{2+}$ model compound.[7, 8] This is a result of the presence of two types of ligands (bpy and $\mathbf{L}_1^{4+}$) involved in the MLCT transitions. The Ru→bpy transitions presumably occur at the same energy as in the model compound, but the transition involving the bpy moiety of $\mathbf{L}_1^{4+}$ occurs at lower energy because of the above-mentioned Coulombic stabilization offered to the MLCT excited state by the positive charges on the paraquat-type units in $\mathbf{L}_1^{4+}$. The MLCT band of $[\{Ru(bpy)_2\}_2\mathbf{L_2}]^{8+}$ occurs at the same wavelength and has an absorption coefficient twice that of $[Ru(bpy)_2\mathbf{L_1}]^{6+}$. This suggests that, as in the case of the Re^{I} complex containing the $\mathbf{L}_2^{4+}$ ligand, the two metal-based moieties do not substantially perturb each other. When the $\mathbf{L}_1^{4+}$ tetracationic cyclophane ligand is replaced by the $\mathbf{L}_4^{4+}$ catenane ligand, the band in the visible region is apparently shifted to lower energy because of the contribution of the CT band present in $\mathbf{L}_4^{4+}$.

In conclusion, the bpy-type moieties of the $\mathbf{L}_1^{4+}$, $\mathbf{L}_2^{4+}$ and $\mathbf{L}_4^{4+}$ ligands behave substantially as simple bpy ligands, but the energy of the MLCT transition involving such ligands is moderately affected by the appended paraquat-type moieties.

Emission spectra of ligands: Among the chromophoric units of the $\mathbf{L}_1^{4+}$, $\mathbf{L}_2^{4+}$, and $\mathbf{L}_4^{4+}$ ligands, only the dioxynaphthalene units of the crown ether are potentially luminescent. In the catenane ligand $\mathbf{L}_4^{4+}$, however, the luminescent excited state of the dioxynaphthalene units is quenched because of the charge-transfer interaction with the paraquat-type units, as previously observed for catenane $\mathbf{2}^{4+}$.[24] Therefore, none of the $\mathbf{L}_1^{4+}$, $\mathbf{L}_2^{4+}$, and $\mathbf{L}_4^{4+}$ ligands exhibits luminescence.

Emission spectra of complexes: The $[Re(CO)_3(Cl)(bpy)]$ and $[Ru(bpy)_3]^{2+}$ model compounds (Table 4) are known to luminesce relatively strongly, both in fluid solution at room temperature and in a rigid matrix at 77 K, from the lowest triplet metal-to-ligand charge-transfer (^{3}MLCT) excited state.[7, 8, 11] None of the complexes examined emits at room temperature. This result is expected, since it is well known that paraquat-type units can quench the luminescent excited state of Re and Ru polypyridine complexes by electron transfer.[11] In a rigid matrix at 77 K, where electron transfer is prevented,[26] emission can be observed from the complexes containing the $\mathbf{L}_1^{4+}$ and $\mathbf{L}_2^{4+}$ ligands (Figures 9 and 10, insets), but not from those containing the catenane ligand $\mathbf{L}_4^{4+}$ (Table 4). This situation shows that, in $[Ru(bpy)_2\mathbf{L_4}]^{6+}$ and $[Re(CO)_3\mathbf{L_4}Cl]^{4+}$, the ^{3}MLCT excited state is quenched by energy transfer to the low-energy CT excited state of the catenane moiety. For the Re and Ru complexes of the $\mathbf{L}_1^{4+}$ and $\mathbf{L}_2^{4+}$ ligands, emission is shifted to lower energies compared with the emission of the $[Re(CO)_3(Cl)(bpy)]$ and $[Ru(bpy)_3]^{2+}$ model compounds (Table 4) because of the stabilizing effect of the positive charges of the paraquat-type units on the ^{3}MLCT excited state. It can also be noted that the emission of $[\{Re(CO)_3Cl\}_2\mathbf{L_2}]^{4+}$ is slightly red-shifted compared to that of $[Re(CO)_3\mathbf{L_1}Cl]^{4+}$. For both the Re and Ru complexes containing the $\mathbf{L}_1^{4+}$ and $\mathbf{L}_2^{4+}$ ligands, the emission lifetime is close to that of the corresponding model compound.

In conclusion, even from the viewpoint of the emission properties, the bpy-type moieties of the $\mathbf{L}_1^{4+}$, $\mathbf{L}_2^{4+}$, and $\mathbf{L}_4^{4+}$ ligands behave substantially as simple bpy ligands, but the appended paraquat-type moieties in $\mathbf{L}_1^{4+}$ and $\mathbf{L}_2^{4+}$ and the CT catenane interaction in $\mathbf{L}_4^{4+}$ play an important role. Particularly worth noting, in view of the possible use of these compounds in photodriven mechanical systems,[6d] is the photoinduced electron-transfer process taking place at room temperature from the ^{3}MLCT excited state to a paraquat-type unit in the $[Re(CO)_3\mathbf{L_1}Cl]^{4+}$, $[\{Re(CO)_3Cl\}_2\mathbf{L_2}]^{4+}$, $[Ru(bpy)_2\mathbf{L_1}]^{6+}$, and $[\{Ru(bpy)_2\}_2\mathbf{L_2}]^{8+}$ complexes.

Electrochemistry of ligands: The electrochemical data for the ligands $\mathbf{L}_1^{4+}$, $\mathbf{L}_2^{4+}$ and $\mathbf{L}_4^{4+}$ are gathered in Table 5. Figure 11 shows schematically the relationships of the processes occurring for $\mathbf{L}_1^{4+}$ and $\mathbf{L}_4^{4+}$. All the potential values are referred to the SCE electrode.

In the case of $\mathbf{L}_1^{4+}$, two reversible bielectronic processes are observed at -0.29 and -0.73 V, followed by a process (-2.10 V) near the end of the accessible potential window. The first and second processes can be assigned to the first and second simultaneous monoelectronic reductions of the two paraquat-type units. The observed potentials are almost the same as those found for the previously investigated tetracationic cyclobis(paraquat-*p*-phenylene).[18, 23] The third process

Table 5. Electrochemical data for ligands and complexes.[a]

	E_{red} (V)	E_{ox} (V)
$\mathbf{L_1}^{4+}$	-0.29;[b] -0.73;[b] -2.10	–
$\mathbf{L_4}^{4+}$	-0.31; -0.49; -0.79; -0.86	$+1.36$;[c] $+1.63$[c]
$\mathbf{L_2}^{4+}$	-0.29;[b] -0.68;[b] -2.03; -2.17	–
$[Re(CO)_3(bpy)(Cl)]$[d]	-1.32	$+1.36$
$[Re(CO)_3\mathbf{L_1}Cl]^{4+}$	-0.28;[b] -0.70;[b] -1.33	$+1.43$; $+1.86$[c]
$[Re(CO)_3\mathbf{L_4}Cl]^{4+}$	-0.27; -0.43; -0.82;[b] -1.40	$+1.33$;[c] $+1.40$;[c] $+2.04$[c]
$[Ru(bpy)_3]^{2+}$	-1.33; -1.52; -1.78	$+1.29$
$[Ru(bpy)_2\mathbf{L_1}]^{6+}$	-0.28;[b] -0.69;[b] -1.32; -1.51; -1.77	$+1.37$
$[Ru(bpy)_2\mathbf{L_4}]^{6+}$	-0.28; -0.44; -0.83;[b] -1.31; -1.52; -1.78	$+1.37$; $+1.54$[c]
$[\{Re(CO)_3Cl\}_2\mathbf{L_2}]^{4+}$	-0.27;[b] -0.62;[b] -1.31;[b]	$+1.42$[b]
$[\{Ru(bpy)_2\}_2\mathbf{L_2}]^{8+}$	-0.28;[b] -0.62;[b] -1.29;[b] ≈ -1.5[e]	$+1.37$[b]

[a] Argon-purged MeCN solution, 298 K; halfwave potential values in V vs SCE; reversible and monoelectronic processes, unless otherwise noted. [b] Bielectronic process. [c] Not fully reversible; potential values estimated from DPV peaks. [d] See ref. [25b]. [e] Affected by adsorption phenomena.

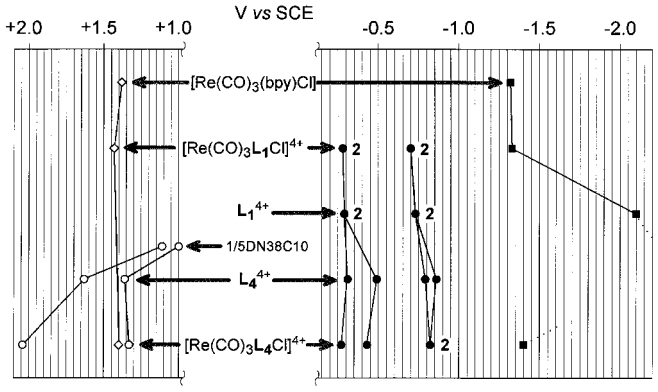

Figure 11. Genetic diagram of the redox potentials of the $\mathbf{L_1}^{4+}$ cyclophane ligand, the $\mathbf{L_4}^{4+}$ catenane ligand, and of their Re^{I} complexes. For comparison purposes, the redox potentials of the $[Re(CO)_3(Cl)(bpy)]$ model compound and of the crown ether 1/5DN38C10, which is a component of $\mathbf{L_4}^{4+}$, are also shown. Solid symbols correspond to reduction processes centered on the paraquat- (●) and the bipyridine-type (■) units. Empty symbols correspond to oxidation processes centered on the Re^{I} metal ion (◇) and the 1/5DMN units (○).

is due to the reduction of the bpy-type unit (-2.09 V in DMF at $-54\,^{\circ}C$ for 2,2′-bipyridine).[27] For the $\mathbf{L_2}^{4+}$ ligand, which contains two paraquat-type and two bpy-type units, four processes are observed. The first two reversible processes (-0.29 and -0.68 V) are bielectronic in nature and can be straightforwardly assigned to the first and second simultaneous monoelectronic reductions of the two paraquat-type units. The third and fourth processes (at -2.03 and about -2.2 V, respectively) can be assigned to the reduction of the two equivalent, but apparently interacting, bpy-type units.

Catenane $\mathbf{L_4}^{4+}$ is formed by the interlocking of two components, the $\mathbf{L_1}^{4+}$ tetracationic cyclophane and the 1/5DN38C10 macrocyclic polyether. The latter component displays two not fully reversible oxidation processes at $+1.00$ and $+1.15$ V, showing that there is some interaction between the two equivalent 1/5DMN units. In the catenane, $\mathbf{L_1}^{4+}$-localized reduction and 1/5DN38C10-localized oxidation processes are expected to occur. In addition, considering the perturbations caused by the charge-transfer interaction, which also induces topological differences between the two paraquat-type units of the cyclophane and the two 1/5DMN units of the crown ether, one expects i) the shift of the reduction processes to more negative potentials and of the oxidation processes to more positive potentials, and ii) the splitting of the degenerate reduction waves of $\mathbf{L_1}^{4+}$. The observed behavior (Table 5 and Figure 11) is fully consistent with the above expectations and with the behavior of the analogous catenane $\mathbf{2}^{4+}$.[24, 28] Specifically, on reduction, the first and third processes can be assigned to the first and second reduction of the alongside paraquat-type unit, whereas the second and fourth processes concern the first and second reduction of the inside unit. On oxidation, the two processes concern oxidation of the alongside and inside electron-donor 1/5DMN units, respectively. The reduction of the bpy moiety (-2.10 V for $\mathbf{L_1}^{4+}$) cannot be observed in $\mathbf{L_4}^{4+}$, suggesting that, when the paraquat-type units have been reduced twice and therefore cannot play a role as electron acceptors, the electron-donor moieties of the crown can be involved in a charge-transfer interaction with the bpy unit.

Electrochemistry of complexes: We have examined the electrochemical behavior of complexes $[Re(CO)_3\mathbf{L_1}Cl]^{4+}$, $[Re(CO)_3\mathbf{L_4}Cl]^{4+}$, $[\{Re(CO)_3Cl\}_2\mathbf{L_2}]^{4+}$, $[Ru(bpy)_2\mathbf{L_1}]^{6+}$, $[Ru(bpy)_2\mathbf{L_4}]^{6+}$, and $[\{Ru(bpy)_2\}_2\mathbf{L_2}]^{8+}$. The results are listed in Table 5, where the data of the $[Re(CO)_3(Cl)(bpy)]$ and $[Ru(bpy)_3]^{2+}$ model compounds are also shown for comparison purposes. Figure 11 shows schematically the relationships of the processes occurring for the $\mathbf{L_1}^{4+}$ and $\mathbf{L_4}^{4+}$ ligands and for their Re complexes, while Figure 12 shows the cyclic voltammetric behavior on reduction of $[Ru(bpy)_2\mathbf{L_4}]^{6+}$. Previous investigations on Re^{I} and Ru^{II} polypyridine complexes have shown that, to a first approximation, the electrochemical processes can be discussed on the basis of localized molecular orbital configurations.[7–11]

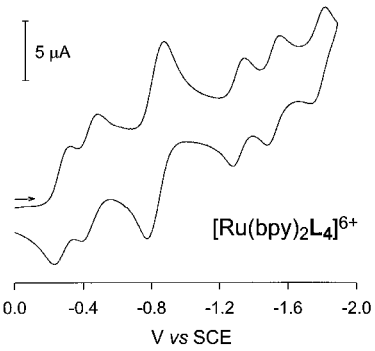

Figure 12. Cyclic voltammetric behavior on reduction of 5×10^{-4} M $[Ru(bpy)_2\mathbf{L_4}]^{6+}$ (acetonitrile solution, 298 K, potential values vs. SCE, scan rate 50 mV s^{-1}, glassy carbon as working electrode, 0.05 M Et_4NPF_6 as supporting electrolyte).

$[Re(CO)_3\mathbf{L_1}Cl]^{4+}$ (Figure 11) shows three reduction and one oxidation processes. The first two (bielectronic) reduction

0947-6539/98/0404-0600 $ 17.50+.50/0 *Chem. Eur. J.* **1998**, *4*, No. 4

processes can be straightforwardly assigned to the first and second simultaneous monoelectronic reductions of the two paraquat-type units of the $\mathbf{L}_1^{4+}$ ligand. These waves are slightly displaced toward less negative potentials compared with uncoordinated $\mathbf{L}_1^{4+}$. The only sizeable difference is the 30 mV displacement of the second reduction wave to less negative values. This displacement can perhaps be attributed to some electron donation of the bireduced paraquat-type units to the coordinated bpy moiety. The following (monoelectronic) wave can be assigned to the reduction of the bpy moiety which, because of metal coordination, becomes much easier to reduce. This process occurs practically at the same potential as for the bpy ligand of the $[Re(CO)_3(Cl)(bpy)]$[25b] model compound showing that, once the paraquat units have been reduced twice, the $\mathbf{L}_1^{4+}$ ligand (now reduced to $\mathbf{L_1}$) behaves like a simple bpy ligand. On the oxidation side, $[Re(CO)_3\mathbf{L_1}(Cl)]^{4+}$ exhibits the expected one-electron wave because of metal oxidation, displaced by 70 mV toward more positive potentials compared with $[Re(CO)_3(Cl)(bpy)]$.[25b] This displacement can be attributed to the presence of a substituted bpy ligand like $\mathbf{L}_1^{4+}$, which is also responsible for the positive charge of the complex.

In the case of $[Ru(bpy)_2\mathbf{L_1}]^{6+}$ as many as six reversible redox processes are observed. As in the case of the analogous Re compound, the first two (bielectronic) reduction processes can again be assigned to the first and second simultaneous monoelectronic reductions of the two paraquat-type units of the $\mathbf{L}_1^{4+}$ ligand, slightly displaced toward less negative potentials compared with uncoordinated $\mathbf{L}_1^{4+}$ (40 mV for the second reduction process). The three following (monoelectronic) waves can be assigned to the successive one-electron reduction of the three bpy moieties. These three processes occur practically at the same potentials as in the $[Ru(bpy)_3]^{2+}$ model compound, showing once again that, after reduction of the paraquat units, the cyclophane ligand behaves as a simple bpy ligand. On the oxidation side, $[Ru(bpy)_2\mathbf{L_1}]^{6+}$ exhibits the one-electron wave due to metal oxidation, displaced by 80 mV toward more positive potentials compared with $[Ru(bpy)_3]^{2+}$. This displacement can be attributed to the large increase in the positive charge of the complex caused by the tetracationic $\mathbf{L}_1^{4+}$ ligand.

The electrochemical behavior of the $[Re(CO)_3\mathbf{L_4}(Cl)]^{4+}$ (Figure 11) and $[Ru(bpy)_2\mathbf{L_4}]^{6+}$ complexes, which contain the $\mathbf{L}_4^{4+}$ catenane ligand, is very interesting. In the accessible potential window, $[Re(CO)_3\mathbf{L_4}(Cl)]^{4+}$ can lose three and accept five electrons and $[Ru(bpy)_2\mathbf{L_4}]^{6+}$ can lose three and accept seven electrons. According to these expectations, the reduction of the two complexes shows two monoelectronic waves and one bielectronic wave involving the paraquat-type units, followed by the monoelectronic reduction waves of the bpy moieties—one for $[Re(CO)_3\mathbf{L_4}Cl]^{4+}$ and three for $[Ru(bpy)_2\mathbf{L_4}]^{6+}$ (Figure 12). For both complexes, the first and second reduction waves of the paraquat units are displaced toward less negative potentials compared with the free ligand $\mathbf{L}_4^{4+}$ (also compared with free $\mathbf{L}_1^{4+}$). These displacements suggest that the charge-transfer interaction between the paraquat units of $\mathbf{L}_1^{4+}$ and 1/5DN38C10 weakens upon coordination. This outcome could be due to i) structural constraints (imposed by the metal coordination of the bpy unit of $\mathbf{L}_4^{4+}$) that prevent optimization of the charge-transfer interaction in the coordinated catenane, and/or ii) the increased electron-acceptor character of the bpy moiety upon coordination, which could partially compete with the paraquat units for the electron donor units of the crown ether. The presence of structural constraints could also account for the fact that the second reduction of the two paraquat units of the coordinated catenane occurs at the same potential, contrary to what happens with the uncoordinated catenane. For $[Re(CO)_3\mathbf{L_4}Cl]^{4+}$, the reduction potential of the bpy-type unit of $\mathbf{L}_4^{4+}$ is clearly displaced toward more negative potentials compared with that of $[Re(CO)_3\mathbf{L_1}(Cl)]^{4+}$, an effect most likely due to the interaction of the coordinated bpy moiety with the electron-donating units of 1/5DN38C10, which is expected to become stronger once the paraquat units have been reduced (vide supra). For $[Ru(bpy)_2\mathbf{L_4}]^{6+}$, the reduction of the three bpy moieties (i.e., the two bpy ligands and the bpy-type unit of $\mathbf{L}_4^{4+}$ in an unknown sequence) occurs at almost the same potentials, just as it does in the case of $[Ru(bpy)_2\mathbf{L_1}]^{6+}$

Upon oxidation, $[Re(CO)_3\mathbf{L_4}(Cl)]^{4+}$ and $[Ru(bpy)_2\mathbf{L_4}]^{6+}$ are expected to exhibit a reversible metal-centered process and two not fully reversible processes involving the 1/5DMN moieties of the crown ether component of the $\mathbf{L}_4^{4+}$ catenane. $[Re(CO)_3\mathbf{L_4}(Cl)]^{4+}$ actually undergoes three not fully reversible processes (Table 5). Comparison with the behavior of $\mathbf{L}_4^{4+}$ and $[Re(CO)_3\mathbf{L_1}(Cl)]^{4+}$ suggests that the first process is due to the oxidation of the alongside 1/5DMN unit of the catenane ligand and the second process to oxidation of the metal. The oxidation of the alongside 1/5DMN unit does not affect the potential of metal oxidation, but compromises its reversibility because of the partial overlap of the two waves. The third process can be assigned to the oxidation of the inside 1/5DMN unit of the catenane ligand. $[Ru(bpy)_2\mathbf{L_4}]^{6+}$ undergoes only two processes. The first process, being reversible, is assigned to the oxidation of the metal center, and the second one, not fully reversible, to the oxidation of the alongside 1/5DMN unit. Such a wave is displaced toward more positive potentials, indicating that oxidation of the metal affects the oxidation of the external 1/5DMN unit presumably because of a change in the structure of the catenane caused by an increased electron donation of the bpy moiety to the oxidized metal. The oxidation of the inside 1/5DMN unit of the crown is displaced outside the accessible potential window. It should also be noted that at this stage the complex has a very large (8+) positive charge, so that further oxidation becomes very difficult.

All the electrochemical processes observed for the binuclear complexes $[\{Re(CO)_3(Cl)\}_2\mathbf{L_2}]^{4+}$ and $[\{Ru(bpy)_2\}_2\mathbf{L_2}]^{8+}$ are bielectronic in nature (Table 5), showing that i) the two paraquat- and two bpy-type units of the $\mathbf{L}_2^{4+}$ ligand behave almost independently, and ii) the two metal-based moieties bridged by $\mathbf{L}_2^{4+}$ largely ignore each other. Thus, one expects to observe three reduction waves and one oxidation wave for the Re complex, and five reduction waves and one oxidation wave for the Ru complex. In the case of $[\{Re(CO)_3Cl\}_2\mathbf{L_2}]^{4+}$, the four expected processes are observed. On the reduction side, the first two processes are due to the first and second simultaneous monoelectronic reduction of the two paraquat-

type units of the bridging ligand, slightly displaced (60 mV for the second reduction) toward less negative potentials compared with uncoordinated $\mathbf{L}_2^{4+}$. The successive reduction process, due to the bpy moieties of the $\mathbf{L}_2^{4+}$ bridge, is very close to the reduction process involving the bpy ligand of the model compound. The simultaneous oxidation of the two Re centers is displaced (60 mV) toward more positive potentials compared with the model compound, that is, at practically the same potential as for $[Re(CO)_3\mathbf{L_1}(Cl)]^{4+}$. In the case of $[\{Ru(bpy)_2\}_2\mathbf{L_2}]^{8+}$, only four reduction waves were observed. The first two processes are again due to the first and second simultaneous monoelectronic reductions of the two paraquat-type units of the $\mathbf{L}_2^{4+}$ ligand, slightly displaced toward less negative potentials compared with uncoordinated $\mathbf{L}_2^{4+}$. The following wave (-1.29 V) can be assigned to the simultaneous one-electron reduction of two bpy moieties (either two bpy ligands coordinated to different metals, or the bpy-type units of the $\mathbf{L}_2^{4+}$ bridge). The fourth process at about -1.5 V is affected by adsorption phenomena, which also preclude observation of the other expected reduction processes. On oxidation, a bielectronic process takes place at the same potential as for the one-electron oxidation of the mononuclear $[Ru(bpy)_2\mathbf{L_1}]^{6+}$ compound.

In conclusion, the electrochemical behavior of the various redox active units present in the $\mathbf{L}_1^{4+}$, $\mathbf{L}_2^{4+}$, and $\mathbf{L}_4^{4+}$ ligands and their complexes can be illustrated on the basis of Figure 11, which explicitly refers to the $\mathbf{L}_1^{4+}$ and $\mathbf{L}_4^{4+}$ ligands and their $[Re(CO)_3\mathbf{L_1}(Cl)]^{4+}$ and $[Re(CO)_3\mathbf{L_4}(Cl)]^{4+}$ complexes. In going from the cyclophane $\mathbf{L}_1^{4+}$ to the catenane $\mathbf{L}_4^{4+}$, the charge-transfer interaction and the fact that the two paraquat-type units of the cyclophane and the two 1/5 DMN units of the crown ether are no longer topologically equivalent i) shift the reduction processes to more negative potentials and the oxidation processes to more positive potentials, and ii) split the two degenerate reductions of $\mathbf{L}_1^{4+}$ into four separated processes. On going from free $\mathbf{L}_1^{4+}$ to its metal complexes, the reduction potentials of the paraquat-type units are scarcely affected, while that of the bpy moiety, which is directly involved in the metal coordination, moves a long way toward less negative values. In the $\mathbf{L}_1^{4+}$ complexes, metal oxidation occurs at practically the same values as in the respective model compounds, indicating that the presence of the two paraquat-type units is of no relevance to this process. The changes observed in going from the free catenane ligand $\mathbf{L}_4^{4+}$ to its complexes are different from those observed in the case of $\mathbf{L}_1^{4+}$, suggesting that the catenane structure changes upon coordination. The most noticeable feature is the lack of splitting of the second reduction of the two paraquat-type units. Comparison between the complexes of the $\mathbf{L}_1^{4+}$ and $\mathbf{L}_4^{4+}$ ligands shows that the metal-centered oxidation occurs at practically the same potential, indicating that the presence of the crown ether does not affect metal oxidation. We can also note that oxidation of the metal and of the alongside 1/5DMN unit of the catenane ligand $\mathbf{L}_4^{4+}$ occur at comparable potentials. The results obtained show that oxidation of the alongside 1/5DMN unit of the $\mathbf{L}_4^{4+}$ ligand does not affect the subsequent oxidation of the metal (in $[Re(CO)_3\mathbf{L_4}(Cl)]^{4+}$), whereas oxidation of the metal affects the successive oxidation of this unit (in $[Ru(bpy)_2\mathbf{L_4}]^{6+}$). Furthermore, we notice that the oxidation of the inside 1/5DMN unit, which occurs after metal oxidation, is strongly displaced toward more positive potentials (400 mV for $[Re(CO)_3\mathbf{L_4}(Cl)]^{4+}$, and outside the examined potential window for $[Ru(bpy)_2\mathbf{L_4}]^{6+}$).

Conclusions

We have synthesized the tetracationic cyclophanes $\mathbf{L}_1^{4+}$ and $\mathbf{L}_2^{4+}$, which contain paraquat-type units together with one and two 2,2′-bipyridine moieties, respectively, as binding sites for the coordination of transition metals. $\mathbf{L}_1^{4+}$ has also been used to obtain the [2]catenanes $\mathbf{L}_3^{4+}$ and $\mathbf{L}_4^{4+}$, made of the tetracationic cyclophane and the macrocyclic polyethers BPP34C10 and 1/5DN38C10, respectively. The $\mathbf{L}_1^{4+}$ and $\mathbf{L}_2^{4+}$ cyclophanes and the $\mathbf{L}_4^{4+}$ [2]catenane ligands have then been used to synthesize novel mono- and binuclear ruthenium(II), rhenium(I), silver(I), and copper(I) complexes.

The $\mathbf{L}_1^{4+}$, $\mathbf{L}_2^{4+}$, and $\mathbf{L}_4^{4+}$ ligands and their $[Re(CO)_3\mathbf{L_1}(Cl)]^{4+}$, $[Re(CO)_3\mathbf{L_4}(Cl)]^{4+}$, $[\{Re(CO)_3(Cl)\}_2\mathbf{L_2}]^{4+}$, $[Ru(bpy)_2\mathbf{L_1}]^{6+}$, $[Ru(bpy)_2\mathbf{L_4}]^{6+}$, and $[\{Ru(bpy)_2\}_2\mathbf{L_2}]^{8+}$ complexes display several redox processes that can be assigned to reduction or oxidation of specific redox-active units: i) reduction of the paraquat- and bpy-type moieties of the cyclophane or catenane ligands, ii) reduction of the bpy ligands (in the Ru complexes), iii) oxidation of the metal (in the Ru and Re complexes) and iv) oxidation of the dioxynaphthalene moieties of the 1/5DN38C10 crown ether (in the $\mathbf{L}_4^{4+}$ ligand and in its complexes).

The $\mathbf{L}_1^{4+}$, $\mathbf{L}_2^{4+}$, and $\mathbf{L}_4^{4+}$ ligands and their $[Re(CO)_3\mathbf{L_1}Cl]^{4+}$, $[Re(CO)_3\mathbf{L_4}Cl]^{4+}$, $[\{Re(CO)_3Cl\}_2\mathbf{L_2}]^{4+}$, $[Ru(bpy)_2\mathbf{L_1}]^{6+}$, $[Ru(bpy)_2\mathbf{L_4}]^{6+}$, and $[\{Ru(bpy)_2\}_2\mathbf{L_2}]^{8+}$ complexes exhibit the absorption bands of their chromophoric subunits. Unlike the $[Ru(bpy)_3]^{2+}$ and $[Re(CO)_3(Cl)(bpy)]$ model compounds, the Ru^{II} and Re^{I} complexes do not exhibit any MLCT luminescence at room temperature because of an electron-transfer quenching process caused by the paraquat-type units of the $\mathbf{L}_1^{4+}$, $\mathbf{L}_2^{4+}$, and $\mathbf{L}_4^{4+}$ ligands. In a rigid matrix at 77 K, where electron transfer cannot occur, emission is observed from the complexes containing the tetracationic cyclophane ligands $\mathbf{L}_1^{4+}$ and $\mathbf{L}_2^{4+}$, but not from those containing the catenane ligand $\mathbf{L}_4^{4+}$, where quenching can still occur by energy transfer to the low-energy CT excited state.

The photoinduced electron-transfer process taking place at room temperature from the ^{3}MLCT excited state to a paraquat-type unit in the $[Re(CO)_3\mathbf{L_1}(Cl)]^{4+}$, $[\{Re(CO)_3(Cl)\}_2\mathbf{L_2}]^{4+}$, $[Ru(bpy)_2\mathbf{L_1}]^{6+}$, and $[\{Ru(bpy)_2\}_2\mathbf{L_2}]^{8+}$ complexes could be useful in the design of new types of photodriven molecular machines.

Experimental Section

Materials and methods: Solvents were purified and dried by literature methods.[29] Reagents were purchased from Aldrich and used as received. BPP34C10,[18] 1/5DN38C10,[30] 1,1′-[phenylenebis(methylene)]bis-4,4′-bipyridinium bis(hexafluorophosphate)[31] ($\mathbf{6}\cdot 2PF_6$), tetrakis(acetonitrile) copper(I) hexafluorophosphate,[32] and 4,4′-bis(hydroxymethyl)-2,2′-bipyridine[17] were prepared as described in the literature. Reactions requiring ultrahigh pressures were carried out in a Teflon vessel by means of a

0947-6539/98/0404-0602 $ 17.50+.50/0 *Chem. Eur. J.* **1998**, *4*, No. 4

custom-built ultrahigh-pressure press, manufactured by PSIKA Pressure Systems of Glossop (UK). Thin-layer chromatography (TLC) was carried out on aluminum sheets precoated with silica gel 60 F (Merck 5554) or with alumina 60 (Merck 5550). The plates were inspected by UV light and developed with iodine vapor. Flash column chromatography was performed on silica gel H (5–40 μm, Fluka 60770) with the solvents specified. Analytical samples were dried in vacuo (0.1 Torr) at 60–70 °C. Melting points were determined on an Electrothermal 9200 apparatus and are not corrected. ^{1}H NMR spectra were recorded on a Joel 270 (270 MHz), a Bruker AC300 (300 MHz), or a Bruker AMX400 (400 MHz) spectrometer with either the solvent or TMS as internal standard. ^{13}C NMR spectra were recorded on Jeol 270, Bruker AC300, or a Bruker AMX400 spectrometer at either 67.5, 75.5, or 100.0 MHz, respectively, using the JMOD pulse sequence, with either the solvent or TMS as internal standard. All chemical shifts are quoted on the δ scale. Electron impact (EI) mass spectra were recorded at 70 eV on a VG ProSpec mass spectrometer. Low-resolution liquid secondary ion mass spectra (LSIMS) were obtained using a VG ZabSpec mass spectrometer equipped with a cesium ion source operating at $\approx$30 keV. The matrix used was *m*-nitrobenzyl alcohol and the scan rate 5 s per decade. High-resolution mass spectra were obtained from the ZabSpec in narrow range voltage scanning mode at $\approx$6000 resolution and employing a cesium/rubidium iodide reference mixture. Microanalyses were performed by the University of Birmingham and the University of North London Microanalytical Service. The equipment and procedures used for the absorption, emission, and electrochemical measurements have been described in detail in a previous paper.[24]

4,4′-Dicarboxy-2,2′-bipyridine (**5b**): The compound was prepared as reported in the literature.[16] Yield 92%, m.p. > 350 °C; the ^{1}H NMR spectrum was in accordance with that reported in the literature.[33] The product was used without further purification in the next step.

4,4′-Dimethoxycarbonyl-2,2′-bipyridine (**5c**): The compound was prepared following a literature procedure[17] in 84% yield, m.p. 210–211 °C; ^{1}H NMR (270 MHz, $CDCl_3$, 25 °C, TMS): δ = 4.00 (s, 6H; CH_3), 7.91 (dd, *J* = 4.7, 1.7 Hz, 2H; PyH-5,5′), 8.87 (d, *J* = 4.9 Hz, 2H; PyH-6,6′), 8.96 (s, 2H; PyH-3,3′); $C_{14}H_{12}N_2O_4$ (272.3): calcd C 61.76, H 4.44, N 10.29; found C 61.52, H 4.39, N 10.45.

4,4′-Bis(hydroxymethyl)-2,2′-bipyridine (**5d**): The compound was prepared following a literature procedure[17] in 79% yield, m.p. 170–171 °C; ^{1}H NMR (270 MHz, CD_3SOCD_3, 25 °C): δ = 4.7 (d, *J* = 5.4 Hz, 4H; CH_2), 5.54 (t, *J* = 5.7 Hz, 2H; OH), 7.38 (d, *J* = 5.2 Hz, 2H; PyH-5,5′), 8.41 (s, 2H; PyH-3,3′), 8.61 (d, *J* = 4.9 Hz, 2H; PyH-6,6′); ^{13}C NMR (67.5 MHz, CD_3SOCD_3, 25 °C): δ = 61.8, 117.8, 121.4, 148.9, 152.8, 155.3.

4,4′-Bis(bromomethyl)-2,2′-bipyridine (**5e**): A mixture of the diol **5d** (5.0 g, 0.023 mol) and hydrobromic acid (200 mL, 48%) was heated under reflux for 3 h before being poured onto ice and neutralized with 10 N NaOH. The white suspension was extracted with several portions of EtOAc (700 mL). The combined extracts were dried ($MgSO_4$) and concentrated in vacuo, and the crude product was subjected to flash column chromatography (SiO_2, eluent CH_2Cl_2/EtOAc, 5:1) to afford **5e** (6.5 g, 75%), m.p. 128–129 °C (*n*-hexane/EtOAc); ^{1}H NMR (270 MHz, $CDCl_3$, 25 °C, TMS): δ = 4.48 (s, 4H; CH_2), 7.35 (dd, *J* = 4.9, 1.7 Hz, 2H; PyH-5,5′), 8.44 (s, 2H; PyH-3,3′), 8.67 (dd, *J* = 4.9, 1.7 Hz, 2H; PyH-6,6′); ^{13}C NMR (67.5 MHz, CD_3SOCD_3, 25 °C): δ = 31.6, 120.5, 124.1, 147.7, 149.7, 155.2; MS (70 eV, EI): *m*/*z* (%) = 342 (100) $[M]^+$, 296 (10), 261 (21), 199 (46), 182 (38), 152 (12), 119 (13), 102 (34), 80 (12), 40 (20); $C_{12}H_{10}Br_2N_2$ (342.0): calcd C 42.14, H 2.95, N 8.19; found C 42.12, H 3.04, N 8.51. A second fraction, after recrystallization from *n*-hexane/EtOAc, gave 1.3 g (18%) of 4-bromomethyl-4-hydroxymethyl-2,2′-bipyridine, m.p. 121 °C. ^{1}H NMR (270 MHz, $CDCl_3$, 25 °C, TMS): δ = 4.48 (s, 2H; CH_2Br), 4.81 (s, 2H; CH_2OH), 5.30 (s, 1H; OH), 7.33 (dd, *J* = 4.8, 1.6 Hz, 2H; PyH-5,5′), 8.35 (s, 1H; PyH-3), 8.40 (s, 1H; PyH-3′), 8.63 (dd, *J* = 4.8 Hz, 1.6 Hz, 2H; PyH-6,6′); ^{13}C NMR (67.5 MHz, $CDCl_3$, 25 °C): δ = 30.7; 63.5, 118.6, 121.1, 121.5, 123.7, 147.4, 149.4, 149.6, 151.3, 155.5, 156.7; MS (70 eV, EI): *m*/*z* (%) = 280 (88) $[^{81}Br, M]^+$, 278 (100) $[^{79}Br, M]^+$, 199 (49), 169 (56), 119 (20), 69 (38), 40 (11); $C_{12}H_{11}BrN_2O$ (279.1): calcd C 51.64, H 3.97, N 10.04; found: C 51.80, H 4.11, N 10.16.

1,1′-[4,4′-Bis(methylene)-2,2′-bipyridyl]bis-4,4′-bipyridinium bis(hexafluorophosphate) (**7**·2PF_6): A solution of the dibromide **5e** (2.2 g, 6.4 mmol) in dry MeCN (150 mL) was added dropwise over 2 h to a stirred and refluxing solution of 4,4′-bipyridine (6.0 g, 38.4 mmol) in dry MeCN (70 mL) under an N_2 atmosphere. The reaction mixture was heated under reflux for 2 d and then cooled in an ice bath. The precipitate was filtered off, washed with ice-cooled MeCN and Et_2O and dried. The solid (4.1 g) was dissolved in warm H_2O (400 mL), treated with charcoal, and filtered. The filtrate was cooled to room temperature and then a 50% aqueous solution of NH_4PF_6 was added. The resulting white precipitate was filtered off, washed with H_2O and Me_2CO, and dried in vacuo (70 °C/0.1 Torr) to give 4.5 g (90%) of **7**·2PF_6, m.p. 297–298 °C (decomp.); ^{1}H NMR (400 MHz, CD_3CN, 25 °C): δ = 5.87 (s, 4H; NCH_2), 7.37 (dd, *J* = 5.0, 2.0 Hz, 2H; H-5), 7.79 (dd, *J* = 6.0, 2.0 Hz, 4H; β-CH), 8.36 (d, *J* = 7 Hz, 4H; β'-CH), 8.50 (d, *J* = 2 Hz, 2H; H-3), 8.74 (d, *J* = 5 Hz, 2H; H-6), 8.85 (dd, *J* = 6.0, 2.0 Hz, 4H; α-CH), 8.87 (d, *J* = 7 Hz, 4H; α'-CH); ^{13}C NMR (75.5 MHz, CD_3SOCD_3): δ = 61.8 (CH_2), 120.3, 122.1, 123.8, 126.1, 145.8, 150.4, 151.0 (CH), 140.9, 144.3, 153.2, 155.5 (Cq); MS (LSIMS): *m*/*z* = 639 $[M - PF_6]^+$, 493 $[M - 2PF_6]^+$; $C_{32}H_{26}F_{12}N_6P_2$ (784.5): calcd C 48.99, H 3.34, N 10.71; found C 49.25, H 3.51, N 10.80.

[2]Catenane **8**·4PF_6: The dibromide **5e** (104 mg, 0.31 mmol), **7**·2PF_6 (200 mg, 0.26 mmol) and the macrocyclic polyether **BPP34C10** (273 mg, 0.51 mmol) were dissolved in dry MeCN (30 mL). The solution was stirred at room temperature for 14 d. The red solution was concentrated in vacuo and the residue was purified by flash column chromatography (SiO_2, eluent MeOH/2 M NH_4Cl/$MeNO_2$, 7:2:1) affording, after counterion exchange, **8**·4PF_6 as a red solid (10 mg, 3%). ^{1}H NMR (300 MHz, CD_3COCD_3, 25 °C, TMS): δ = 3.37 (m, 8H; OCH_2), 3.54 (m, 8H; OCH_2), 3.85 (m, 8H; OCH_2), 3.92 (m, 8H; OCH_2), 5.63 (s, 8H; OC_6H_4), 6.22 (s, 8H; NCH_2), 7.91 (d, *J* = 5 Hz, 4H; PyH-5), 8.27 (d, *J* = 7 Hz, 8H; β-CH), 8.38 (s, 4H; PyH-3), 8.82 (d, *J* = 5 Hz, 4H; PyH-6), 9.38 (d, *J* = 7 Hz, 8H; α-CH); MS (FAB): *m*/*z*: 1647 $[M - PF_6]^+$, 1502 $[M - 2PF_6]^+$, 1357 $[M - 3PF_6]^+$.

[3]Catenane **9**·4PF_6: A mixture of **7**·4PF_6 (118 mg, 0.15 mmol), the dibromide **5e** (61 mg, 0.19 mmol), and the macrocyclic polyether **BPP34C10** (161 mg, 0.30 mmol) was warmed until all the solid dissolved. A solution was transferred to a high pressure Teflon cell and subjected to 12 kbar for 3 d at room temperature. The resulting red solution was concentrated in vacuo and the residue was purified by flash column chromatography (SiO_2, eluent MeOH/2 M NH_4Cl/$MeNO_2$, 7:2:1). The fractions containing the catenane were combined and concentrated in vacuo. The solid residue was dissolved in H_2O and treated with an excess of 50% NH_4PF_6 solution. The precipitate was filtered off, washed with H_2O and dried in vacuo (70 °C/0.1 Torr) to afford 7.0 mg (2%) [3]catenane **9**·4PF_6 as a deep red solid. MS (LSIMS): *m*/*z* = 2330 $[M]^+$, 2185 $[M - PF_6]^+$, 2040 $[M - 2PF_6]^+$, 1894 $[M - 3PF_6]^+$, 1647 $[M - PF_6 - CE]^+$, 1502 $[M - 2PF_6 - CE]^+$, 1357 $[M - 3PF_6 - CE]^+$, 1111 $[M - PF_6 - 2CE]^+$, 966 $[M - 2PF_6 - 2CE]^+$, 821 $[M - 3PF_6 - 2CE]^+$; HRMS (LSIMS) $C_{100}H_{116}F_{12}N_8O_{20}P_2$: $[M - 2PF_6]^+$ calcd 2038.7537, found 2038.7590.

Cyclophane $\mathbf{L_1}$·4PF_6: A solution of **6**·2PF_6 (3.53 g, 5.0 mmol) in dry MeCN (150 mL) and a solution of the dibromide **5e** (1.62 g, 5.0 mmol) in dry MeCN (150 mL) were added simultaneously under an atmosphere of N_2 to stirred and refluxing MeCN (300 mL) over a period of 6 h. The reaction mixture was maintained under reflux for 4 d and then concentrated in vacuo. The crude product was purified by flash column chromatography (SiO_2, eluent MeOH/2 M NH_4Cl/$MeNO_2$, 7:2:1). After evaporation of the solvent, the product was dissolved in H_2O and treated with an excess of 50% NH_4PF_6 solution. The precipitate was filtered off, washed with H_2O and dried in vacuo (70 °C/0.1 Torr). Yield 1.12 g (24%), m.p. 268 °C (decomp.). ^{1}H NMR (400 MHz, CD_3CN, 25 °C): δ = 5.77 (s, 4H; xylyl NCH_2), 5.87 (s, 4H; $PyNCH_2$), 7.56 (s, 4H; C_6H_4), 7.88 (dd, *J* = 5.0, 1.0 Hz, 2H; PyH-5), 8.13 (s, 2H; PyH-3), 8.18 (d, *J* = 7 Hz, 4H; β-CH), 8.21 (d, *J* = 7 Hz, 4H; β'-CH), 8.83 (d, *J* = 5 Hz, 2H; PyH-6), 8.86 (d, *J* = 7 Hz, 4H; α-CH), 8.92 (d, *J* = 7 Hz, 4H; α'-CH); ^{13}C NMR (100 MHz, CD_3CN, 25 °C): δ = 64.2, 65.6 (CH_2), 123.9 (C-3), 127.5 (C-5), 128.5 (β-CH), 128.6 (β'-CH), 131.4 (xylyl), 146.2 (α-CH), 146.5 (α'-CH), 150.5 (C-6), 136.7, 150.8, 151.2 (Cq); MS (LSIMS): *m*/*z* = 1033 $[M - PF_6]^+$, 888 $[M - 2PF_6]^+$, 743 $[M - 3PF_6]^+$; $C_{40}H_{34}F_{24}N_6P_4$ (1178.6): calcd C 40.76, H 2.91, N 7.13; found C 40.51, H 2.99, N 6.96.

Cyclophane $\mathbf{L_2}$·4PF_6: A solution of **7**·2PF_6 (0.784 g, 1.0 mmol) in dry MeCN (75 mL) and a solution of the dibromide **5e** (0.324 g, 1.0 mmol) in dry MeCN (75 mL) were added simultaneously under an atmosphere of N_2 to stirred and refluxing MeCN (80 mL) over a period of 4 h. The reaction mixture was maintained under reflux for 4 d and then concentrated in vacuo. The crude product was purified by flash column chromatography (SiO_2, eluent MeOH/2 M NH_4Cl/$MeNO_2$, 7:2:1). After evaporation of the solvent the product was dissolved in water and treated with an excess of 50% NH_4PF_6 solution. The precipitate was filtered off, washed with H_2O,

and dried in vacuo (70 °C/0.1 Torr). Yield 0.31 g (25 %), m.p. > 300 °C; ^{1}H NMR (300 MHz, CD_3SOCD_3, 25 °C): $\delta = 5.97$ (s, 8H; NCH_2), 7.93 (d, $J =$ 5 Hz, 4H; PyH-5), 8.39 (s, 4H; PyH-3), 8.58 (d, $J = 7$ Hz, 8H; β-CH), 8.81 (d, $J = 5$ Hz, 4H; PyH-6), 9.55 (d, $J = 7$ Hz, 8H; α-CH); ^{13}C NMR (75.5 MHz, CD_3SOCD_3, 25 °C): $\delta = 62.3$ (CH_2), 121.6, 125.0, 127.3, 145.4, 150.8 (CH), 144.3, 149.0, 156.2 (Cq); MS (LSIMS): $m/z = 1111$ $[M - PF_6]^+$, 966 $[M - 2PF_6]^+$, 821 $[M - 3PF_6]^+$; $C_{44}H_{34}F_{24}N_8P_4$ (1256.7): calcd C 42.05, H 2.89, N 8.92; found C 42.03, H 2.81, N 8.76.

[2]Catenane $L_3 \cdot 4PF_6$: The dibromide **5e** (40 mg, 0.12 mmol), **6** · $2PF_6$ (75 mg, 0.11 mmol), and the macrocyclic polyether **BPP34C10** (142 mg, 0.27 mmol) were dissolved in dry MeCN (30 mL). The solution was stirred at room temperature for 14 d. The deep red solution was concentrated in vacuo and the residue was purified by flash column chromatography (SiO_2, eluent MeOH/2 M NH_4Cl/$MeNO_2$, 7:2:1) affording, after counterion exchange, $\mathbf{L_3} \cdot 4PF_6$ as a red solid (55 mg, 30 %). M.p. > 250 °C; ^{1}H NMR (300 MHz, CD_3COCD_3, 25 °C, TMS): $\delta = 3.51 - 4.12$ (m, 32H; OCH_2), 5.23 (brs, 8H; OC_6H_4), 6.12 (s, 4H; NCH_2), 6.18 (s, 4H; NCH_2), 7.93 (d, 2H; PyH-5), 8.04 (s, 4H; C_6H_4), 8.12 (m, 8H; β-CH), 8.18 (s, 2H; PyH-3), 8.92 (d, 2H; PyH-6), 9.38 and 9.43 (2 × d, 2 × 4H; α-CH); ^{13}C NMR (75.5 MHz, CD_3COCD_3, 25 °C): $\delta = 64.2$, 65.5, 68.0, 68.7, 70.6, 70.8, 71.3 (CH_2), 123.5, 125.0, 126.7, 126.9, 131.6, 146.0, 146.3, 151.8 (CH), 137.2, 144.2, 148.0, 159.4 (Cq); MS (LSIMS): $m/z = 1570$ $[M - PF_6]^+$, 1424 $[M - 2PF_6]^+$. $C_{68}H_{74}F_{24}N_6O_{10}P_4$ (1712.4): calcd C 47.61, H 4.4.32, N 4.90; found C 47.54, H 4.39, N 4.93.

[2]Catenane $L_4 \cdot 4PF_6$: The dibromide **5e** (150 mg, 0.44 mmol), **7** · $2PF_6$ (282 mg, 0.4 mmol),[4] and the macrocyclic polyether **1/5DN38C10** (127 mg, 0.2 mmol) were dissolved in warm, dry DMF (7 mL). The solution was transferred to an ultrahigh-pressure Teflon reaction vessel, which was then compressed (12 kbar) at 20 °C for 3 d. After decompression of the reaction vessel, the deep red solution was concentrated in vacuo. The residue was purified by flash column chromatography (SiO_2, eluent MeOH/2 M NH_4Cl/$MeNO_2$, 7:2:1). The fractions containing the catenane were combined and concentrated in vacuo. The solid residue was dissolved in H_2O and treated with an excess of 50 % NH_4PF_6 solution. The precipitate was filtered off, washed with H_2O, and dried in vacuo (70 °C/0.1 Torr) to afford 150 mg (41 %) [2]catenane $\mathbf{L_4} \cdot 4PF_6$ as a deep pink solid, m.p. 262 °C (decomp.). ^{1}H NMR (400 MHz, CD_3COCD_3, 243 K, 2D COSY 45): $\delta = 3.29$ (d, 1H; NpH), 3.53 – 4.33 (m, 32H; OCH_2), 4.65 (d, 1H; NpH), 5.38 (t, 1H; NpH), 5.62 (t, 1H; NpH), 5.92 – 6.30 (m, 8H; NCH_2), 6.07 (d, 1H; NpH), 6.18 (d, 1H; NpH), 6.36 (d, 1H; NpH), 6.46 (d, 1H; NpH), 7.00 (m, 3H; NpH and PyH-5), 7.14 (d, 3H; NpH and PyH-5′), 7.33 (brs, 2H; β-CH), 7.69 (brs, 2H; β'-CH), 7.84 (brs, 2H; β-CH), 7.98 (brs, 2H; β-CH), 8.00 (brs, 2H; C_6H_4), 8.15 (brs, 1H; PyH-3), 8.31 (brs, 2H; C_6H_4), 8.38 (brs, 1H; PyH-3′), 8.73 (brs, 1H; PyH-6), 8.79 (brs, 1H; PyH-6′), 9.04 (d, 2H; α-CH), 9.11 (brs, 2H; α-CH), 9.20 (brs, 2H; α-CH), 9.38 (brs, 2H; α-CH); ^{13}C NMR (100 MHz, CD_3COCD_3, 213 K): $\delta = 64.2$, 65.6, 68.1, 68.5, 70.4, 70.6, 71.2, 72.1 (CH_2), 104.6, 105.5, 106.5, 110.2, 111.1, 114.5, 125.3, 125.6, 126.3, 126.9, 131.6, 145.2, 145.5 (CH), 124.6, 124.9, 137.5, 144.0, 152.5, 154.1 (Cq); MS (LSIMS): $m/z = 1814$ $[M]^+$, 1669 $[M - PF_6]^+$, 1524 $[M - 2PF_6]^+$, 1379 $[M - 3PF_6]^+$; $C_{76}H_{78}F_{24}N_6O_{10}P_4$ (1815.4): calcd C 50.28, H 4.33, N 4.63; found C 50.39, H 4.19, N 4.82. Single crystals suitable for X-ray crystallography were grown by vapor diffusion of iPr$_2$O into a 1:1 MeCN/$MeNO_2$ solution of $\mathbf{L_4} \cdot 4PF_6$.

General procedure for synthesis of bis-heteroleptic Ru^{II} complexes $[Ru(bpy)_2L_1](PF_6)_6$, $[Ru(bpy)_2]_2L_2](PF_6)_8$, $[Ru(bpy)_2L_3](PF_6)_6$, $[Ru(bpy)_2L_4](PF_6)_6$: A mixture of $[Ru(bpy)_2Cl_2] \cdot 2H_2O$ and the appropriate ligand ($\mathbf{L_1} \cdot 4PF_6 - \mathbf{L_4} \cdot 4PF_6$) in EtOH/$H_2O$ (3:1, v/v) was heated under reflux under an N_2 atmosphere for 48 h. The solvent was removed in vacuo, and H_2O was added to the residue and filtered (to remove an excess of the ligand). The filtrate was treated with 50 % aqueous solution NH_4PF_6, the resulting precipitate was filtered off, washed with H_2O and Et_2O, and dried in vacuo (60 °C/0.1 Torr). The compounds were further purified by precipitation after vapor diffusion of iPr$_2$O into MeCN solutions of the complexes.

$[Ru(bpy)_2L_1](PF_6)_6$: From $[Ru(bpy)_2Cl_2]$ (73 mg, 0.15 mmol) and $\mathbf{L_1} \cdot 4PF_6$ (194 mg, 0.165 mmol) in EtOH/H_2O (35 mL); yield 222 mg (94 %), m.p. 238 °C (decomp.); ^{1}H NMR (300 MHz, CD_3CN, 25 °C, 2D COSY 45): $\delta =$ 5.79 (s, 4H; xylyl NCH_2), 5.81 (s, 4H; $PyNCH_2$), 7.38 (m, 4H; bpyH-4), 7.63 (s, 4H; C_6H_4), 7.63 – 7.67 (m, 6H; bpyH-3 and PyH-5), 7.90 (d, $J = 6$ Hz, 2H; PyH-6), 8.06 (t, $J = 8$ Hz, 4H; bpyH-5), 8.17 (d, $J = 8$ Hz, 8H; β-CH and β'-CH), 8.33 (s, 2H; PyH-3), 8.50 (d, $J = 8$ Hz, 4H; bpyH-6), 8.84 (d, $J = 7$ Hz, 4H; α-CH), 8.88 (d, $J = 7$ Hz, 4H; α'-CH); ^{13}C NMR (75.5 MHz, CD_3CN, 25 °C): $\delta = 63.2$, 65.7 (CH_2), 125.1, 126.1, 128.4, 128.6, 130.0, 131.4, 18.9, 145.9, 146.4, 152.4, 152.8, 153.7 (CH), 136.8, 141.9, 151.0, 151.3, 157.6, 158.5 (Cq); MS (LSIMS): $m/z = 1737$ $[M - PF_6]^+$, 1592 $[M - 2PF_6]^+$, 1447 $[M - 3PF_6]^+$; $C_{60}H_{50}F_{36}N_{10}P_6Ru$ (1882.0): calcd C 38.29, H 2.68, N 7.44; found C 38.27, H 2.84, N 7.42.

$[\{Ru(bpy)_2\}_2L_2](PF_6)_8$: From $[Ru(bpy)_2Cl_2]$ (53.2 mg, 0.11 mmol) and $\mathbf{L_2} \cdot 4PF_6$ (62.8 mg, 0.05 mmol) in EtOH/H_2O (20 mL); yield 127 mg (97 %), m.p. 240 °C (decomp.); ^{1}H NMR (400 MHz, CD_3CN, 25 °C, 2D COSY 45): $\delta = 5.89$ (s, 8H; NCH_2), 7.39 (m, 8H; bpyH-4), 7.64 (dd, $J = 6.0$, 2.0 Hz; 4H; PyH-5), 7.69 (m, 8H; bpyH-3), 7.89 (d, $J = 6$ Hz, 4H; PyH-6), 8.07 (m, 8H; bpyH-5), 8.28 (d, $J = 7$ Hz, 8H; β-CH), 8.30 (brs, 4H; PyH-3), 8.50 (d, $J =$ 8 Hz, 8H; bpyH-6), 8.96 (d, $J = 7$ Hz, 8H; α-CH); ^{13}C NMR (75.5 MHz, CD_3CN, 25 °C): $\delta = 63.2$ (CH_2), 125.2, 125.6, 128.7, 129.5, 139.0, 146.7, 152.3, 152.7, 153.6 (CH), 142.5, 157.6, 158.4 (Cq); MS (LSIMS): $m/z = 2519$ $[M - PF_6]^+$, 2375 $[M - 2PF_6]^+$, 2229 $[M - 3PF6]^+$; $C_{84}H_{68}F_{48}N_{16}P_8Ru_2$ (2663.4): calcd C 37.88, H 2.57, N 8.41; found C 37.66, H 2.62, N 8.42. Single crystals suitable for X-ray crystallography were obtained by slow evaporation of Me_2CO from a mixture Me_2CO/C_6H_6 solution of the complex.

$[Ru(bpy)_2L_3](PF_6)_6$: From $[Ru(bpy)_2Cl_2]$ (48 mg, 0.03 mmol) and $\mathbf{L_3} \cdot 4PF_6$ (13 mg, 0.03 mmol) in EtOH/H_2O (20 mL); yield 60 mg (82 %). ^{1}H NMR (300 MHz, CD_3COCD_3, 25 °C): $\delta = 3.3 - 4.0$ (m, 36H; OCH_2 + alongside OC_6H_4), 6.12 (s, 4H; NCH_2), 6.24 (brs, 4H; inside OC_6H_4), 6.24 (s, 4H; NCH_2), 7.9 – 8.3 (m, 26H; β-CH and C_6H_4 and PyH), 7.5 – 7.7 (m, 4H; PyH), 8.75 – 8.84 (m, 6H; PyH-6), 8.96 and 9.24 (2 × d, 2 × 4H; α-CH); ^{13}C NMR (75.5 MHz, CD_3COCD_3, 25 °C): $\delta = 63.0$, 65.5, 70.6, 70.8, 70.9 (CH_2), 125.2, 125.4, 125.5, 125.6, 126.3, 126.9, 128.6, 128.8, 128.9, 129.2, 131.5, 131.9, 157.6, 157.8 (CH), 115.8, 139.2, 139.4, 146.7, 152.5, 152.9, 154.5, 157.9, 158.5 (Cq); MS (LSIMS): $m/z = 2273$ $[M - PF_6]^+$, 2128 $[M - 2PF_6]^+$.

$[Ru(bpy)_2L_4](PF_6)_6$: From $[Ru(bpy)_2Cl_2]$ (24.2 mg, 0.05 mmol) and $\mathbf{L_4} \cdot 4PF_6$ (100 mg, 0.054 mmol) in EtOH/H_2O (40 mL); yield 118 mg (82 %); m.p. 201 °C (decomp.); ^{13}C NMR (100 MHz, CD_3CN, 31 °C): $\delta = 62.9$, 66.0, 68.9, 69.1, 69.2, 69.4, 70.2, 70.4, 70.7, 71.1, 71.2, 71.5, 72.0, 72.2, 72.6 (CH_2), 105.5, 106.5, 106.9, 106.9, 110.4, 111.4, 114.7, 115.0, 124.4, 124.5, 125.5, 125.6, 125.6, 125.7, 126.4, 126.6, 127.0, 127.2, 127.7, 128.9, 129.0, 129.1, 131.7, 131.9, 132.0, 139.5, 139.7, 145.0, 146.2, 152.4, 152.4, 152.6, 152.8, 155.1, 155.2 (CH), 137.8, 137.9, 142.4, 153.3, 154.2, 154.8, 157.7, 157.8, 158.0, 158.0, 158.1 (Cq); MS (LSIMS): $m/z = 2373$ $[M - PF_6]^+$, 2229 $[M - 2PF_6]^+$, 2084 $[M - 3PF_6]^+$; $C_{96}H_{94}F_{36}N_{10}O_{10}P_6Ru$ (2518.7): calcd C 45.78, H 3.76, N 5.56; found C 45.87, H 3.85, N 5.49.

General procedure for synthesis of Re^{I} complexes $[Re(CO)_3ClL_1](PF_6)_4$, $[Re(CO)_3Cl]_2L_2](PF_6)_4$, and $[Re(CO)_3ClL_4](PF_6)_4$: A mixture of $[Re(CO)_5Cl]$ and the appropriate ligand ($\mathbf{L_1} \cdot 4PF_6$, $\mathbf{L_2} \cdot 4PF_6$, or $\mathbf{L_4} \cdot 4PF_6$) in anhydrous MeOH was heated under reflux and under an atmosphere of N_2 for 24 h. After cooling in a refrigerator, the yellow precipitate was filtered off, washed with THF and Et_2O, and dried in vacuo.

$[Re(CO)_3ClL_1](PF_6)_4$: From $[Re(CO)_5Cl]$ (80 mg, 0.22 mmol) and $\mathbf{L_1} \cdot 4PF_6$ (236 mg, 0.20 mmol) in of MeOH (25 mL); yield 234 mg (79 %), m.p. 268 °C (decomp.). ^{1}H NMR (300 MHz, CD_3CN, 25 °C): $\delta = 5.79$ (s, 4H; xylyl NCH_2), 5.96 (s, 4H; Py NCH_2), 7.64 (s, 4H; C_6H_4), 7.96 (dd, $J = 6.0$, 2.0 Hz; 2H; PyH-5), 8.22 (d, $J = 7$ Hz, 4H; β-CH), 8.25 (d, $J = 7$ Hz, 4H; β'-CH), 8.94 (d, $J = 7$ Hz, 4H; α-CH), 9.02 (brs, 2H; PyH-3), 9.15 (d, $J = 6$ Hz, 2H; PyH-6), 9.34 (d, $J = 7$ Hz, 4H; α'-CH); ^{13}C NMR (75.5 MHz, CD_3CN, 25 °C): $\delta = 63.4$, 65.7 (CH_2), 126.5, 128.4, 128.6, 130.2, 131.5, 146.0, 147.2, 155.1 (CH), 136.9, 145.1, 151.0, 151.4, 157.2 (Cq), 198.3 (C=O); MS (LSIMS): $m/z = 1339$ $[M - PF_6]^+$, 1194 $[M - 2PF_6]^+$, 1049 $[M - 3PF_6]^+$; $C_{43}H_{34}ClF_{24}O_3P_4Re$ (1484.3): calcd C 34.80, H 2.31, N 5.66; found C 34.61, H 2.24, N 5.87. Single crystals suitable for X-ray crystallography were obtained by vapor diffusion of benzene into a $MeNO_2$ solution of $[Re(CO)_3Cl\mathbf{L_1}](PF_6)_4$.

$[Re(CO)_3Cl]_2L_2](PF_6)_4$: From $[Re(CO)_5Cl]$ (40.0 mg, 0.11 mmol) and $\mathbf{L_2} \cdot 4PF_6$ (64.0 mg, 0.05 mmol) in MeOH (25 mL); yield 62 mg (66 %), m.p. > 300 °C (decomp.); ^{1}H NMR (300 MHz, CD_3SOCD_3, 25 °C): $\delta = 6.12$ (s, 8H; NCH_2), 8.15 (d, $J = 5$ Hz, 4H; PyH-5), 8.73 (d, $J = 5.5$ Hz, 8H; β-CH), 8.89 (brs, 4H; PyH-3), 9.20 (d, $J = 5$ Hz, 4H; PyH-6), 9.59 (d, $J = 6$ Hz, 8H; α-CH); MS (LSIMS): $m/z = 1723$ $[M - PF_6]^+$, 1578 $[M - 2PF_6]^+$, 1433 $[M - 3PF_6]^+$; $C_{50}H_{36}Cl_2F_{24}O_6P_4Re_2$ (1868.1): calcd C 32.15, H 1.94, N 6.00; found C 32.06, H 1.92, N 5.93.

$[Re(CO)_3ClL_4](PF_6)_4$: From $[Re(CO)_5Cl]$ (12.0 mg, 0.033 mmol) and $\mathbf{L_4} \cdot 4PF_6$ (54.4 mg, 0.030 mg) in MeOH (10 mL). After 24 h under reflux, the

0947-6539/98/0404-0604 $ 17.50+.50/0 *Chem. Eur. J.* **1998**, *4*, No. 4

reaction mixture was concentrated in vacuo to about one third of its original volume. Addition of Et_2O precipitated the product, which was treated with 50% aqueous NH_4PF_6, washed with H_2O and dried in vacuo; yield 52.1 mg (82%), m.p. 261 °C (decomp.); ^{1}H NMR (100 MHz, CD_3CN, 313 K, 2D COSY 45): $\delta = 3.08$ (d, 1H; NpH), 3.6–4.2 (m, 32H; OCH_2), 5.7–6.1 (m, 8H; NCH_2), 6.05 (d, 1H; NpH), 6.28 (d, 1H; NpH), 6.38 (d, 1H; NpH), 6.51 (t, 1H; NpH), 6.63 (d, 1H; NpH), 6.95–7.15 (m, 8H; β-CH and β'-CH), 7.02 (t, 1H; NpH), 7.07 (d, 1H; NpH), 7.23 (t, 1H; NpH), 7.31 (d, 1H; NpH), 7.95 (br s, 4H; C_6H_4), 8.01 (d, 2H; PyH-5), 8.27 (br s, 2H; PyH-3), 8.37 (m, 4H; α-CH), 8.74 (m, 4H; α'-CH), 9.36 (d, 2H; PyH-6); MS (LSIMS): $m/z = 2120$ $[M]^+$, 1975 $[M - PF_6]^+$, 1830 $[M - 2PF_6]^+$, 1685 $[M - 3PF_6]^+$; $C_{79}H_{78}ClN_4O_{13}P_4F_{24}$ (2121.0): calcd C 44.74, H 3.71, N 3.96; found C 44.55, H 3.97, N 4.10.

General procedure for synthesis of Ag^I complexes $[Ag(L_1)_2](PF_6)_9$, $[Ag(L_3)_2](PF_6)_9$, and $[Ag(L_4)_2](PF_6)_9$: A solution of silver(I) triflate in dry MeCN was added to a stirred solution of the appropriate ligand ($\mathbf{L_1}\cdot 4PF_6$, $\mathbf{L_3}\cdot 4PF_6$, and $\mathbf{L_4}\cdot 4PF_6$) in dry MeCN under an atmosphere of N_2 at room temperature. After 8 h of stirring in the dark, the solvent was removed in vacuo, and the residue was treated with a 50% aqueous solution of NH_4PF_6. The precipitate was filtered off, washed with H_2O and Et_2O, and dried in vacuo.

$[Ag(L_1)_2](PF_6)_9$: From $\mathbf{L_1}\cdot 4PF_6$ (118 mg, 0.1 mmol) and $AgCF_3SO_3$ (13.0 mg, 0.05 mmol) in 12 mL MeCN; yield 112 mg (82%), m.p. 280 °C (decomp.); ^{1}H NMR (300 MHz, CD_3CN, 25 °C): $\delta = 5.75$ (s, 8H; xylyl NCH_2), 5.83 (s, 8H; $PyNCH_2$), 7.55 (s, 8H; C_6H_4), 7.73 (d, $J = 4$ Hz, 4H; PyH-5), 8.11 (s, 4H; PyH-3), 8.20 (m, 16H; β-CH and β'-CH), 8.76 (d, $J = 5$ Hz, 4H; PyH-6), 8.88 (d, $J = 6.6$ Hz, 8H; α-CH), 9.00 (d, $J = 6.6$ Hz, 8H; α'-CH); ^{13}C NMR (75.5 MHz, CD_3CN, 25 °C): $\delta = 64.1$, 65.4 (CH_2), 123.4, 126.7, 128.3, 128.4, 131.2, 145.9, 146.2, 151.6 (CH), 136.6, 144.2, 150.7, 151.0, 155.7 (Cq); MS (LSIMS): $m/z = 2465$ $[M - PF_6]^+$, 2320 $[M - 2PF_6]^+$, 2212 $[M - Ag - 2PF_6]^+$, 2176 $[M - 3PF_6]^+$, 2067 $[M - Ag - 3PF_6]^+$, 1923 $[M - Ag - 4PF_6]^+$; $C_{80}H_{68}AgF_{54}N_{12}P_9$ (2610.1): calcd C 36.81, H 2.63, N 6.44; found C 36.91, H 2.58, N 6.46. Single crystals suitable for X-ray crystallography were obtained by vapor diffusion of benzene into a MeCN solution of $[Ag(\mathbf{L_1})_2](PF_6)_9$.

$[Ag(L_3)_2](PF_6)_9$: From $\mathbf{L_3}\cdot 4PF_6$ (13 mg, 0.04 mmol) and $AgCF_3SO_3$ (2.1 mg, 0.02 mmol) in MeCN (10 mL); yield 72 mg (93%); ^{1}H NMR (300 MHz, CD_3CN, 25 °C): $\delta = 3.44$–3.92 (m, 36H; OCH_2 and inside OC_6H_4), 6.10 (s, 4H; NCH_2), 6.25 (br s, 4H; alongside OC_6H_4), 6.39 (s, 4H; NCH_2), 7.99 (m, 6H; C_6H_4 and PyH-4), 8.15 (m, 8H; β-CH), 8.65 (s, 2H; PyH-6), 9.18 (d, 2H; PyH-3), 9.00 and 9.32 (2 × d, 2 × 4H; α-CH); ^{13}C NMR (75.5 MHz, CD_3COCD_3, 25 °C): $\delta = 63.3$, 65.5, 70.6, 70.9, 71.3, 73.7 (CH_2), 118.4, 120.9, 131.6, 137.3, 139.2, 141.5, 146.1, 146.4, 147.4 (CH), 148.6, 148.7, 150.7, 151.5 (Cq); MS (LSIMS): $m/z = 3538$ $[M - 2PF_6]^+$, 3393 $[M - 2PF_6]^+$, 3248 $[M - 3PF_6]^+$, 3103 $[M - 4PF_6]^+$.

$[Ag(L_4)_2](PF_6)_9$: From $\mathbf{L_4}\cdot 4PF_6$ (72.6 mg, 0.04 mmol) and $AgCF_3SO_3$ (5.1 mg, 0.02 mmol) in MeCN (10 mL); yield 72 mg (93%), m.p. 267 °C (decomp.); ^{13}C NMR (100 MHz, CD_3CN, 31 °C): $\delta = 64.4$, 65.9, 68.9, 70.8, 71.3, 72.1 (CH_2), 106.8, 114.8, 123.6, 125.6, 125.8, 126.3, 1216.8, 131.8, 145.2, 145.5, 152.6 (CH_2), 137.5, 144.0, 159.2 (Cq); MS (LSIMS): $m/z = 3485$ $[M - Ag - 2PF_6]^+$, 3340 $[M - Ag - 3PF_6]^+$, 3195 $[M - Ag - 4PF_6]^+$, 3051 $[M - Ag - 5PF_6]^+$; $C_{152}H_{156}AgF_{54}N_{12}O_{20}P_9$ (3883.5): calcd C 47.01, H 4.05, N 4.33; found C 46.85, H 4.12, N 4.43.

General procedure for synthesis Cu^I complexes $[Cu(L_1)_2](PF_6)_9$ and $[Cu(L_4)_2](PF_6)_9$: A solution of $[Cu(MeCN)_4]PF_6$ in dry MeCN was added by means of a syringe to a stirred solution of the appropriate ligand ($\mathbf{L_1}\cdot 4PF_6$ or $\mathbf{L_4}\cdot 4PF_6$) in dry MeCN under an atmosphere of N_2 in a Schlenk flask at room temperature. The solution immediately became brown. After 4 h, the solution was concentrated in vacuo to about a third of its volume. Addition of Et_2O precipitated the product, which was filtered off, washed with Et_2O, and dried in vacuo.

$[Cu(L_1)_2](PF_6)_9$: From $\mathbf{L_1}\cdot 4PF_6$ (118.0 mg, 0.1 mmol) and $[Cu(MeCN)_4]PF_6$ (18.0 mg, 0.05 mmol) in MeCN (10 mL); yield 106 mg (83%), m.p. 239 °C (decomp.); ^{1}H NMR (300 MHz, CD_3SOCD_3, 25 °C): $\delta = 5.83$ (s, 8H; xylyl NCH_2), 5.92 (s, 8H; $PyNCH_2$), 7.67 (s, 8H; C_6H_4), 7.90 (s, 4H; PyH-5), 8.24 (s, 4H; PyH-3), 8.59 (br s, 16H; β-CH and β'-CH), 8.77 (s, 4H; PyH-6), 9.44 (br s, 8H; α-CH), 9.51 (s, 8H; α'-CH); MS (LSIMS): $m/z = 2420$ $[M - PF_6]^+$, 2274 $[M - 2PF_6]^+$, 2130 $[M - 3PF_6]^+$; $C_{80}H_{68}CuF_{54}N_{12}P_9$ (2565.7): calcd C 37.45, H 2.67, N 6.55; found C 37.67, H 2.51, N 6.72.

$[Cu(L_4)_2](PF_6)_9$: From $\mathbf{L_4}\cdot 4PF_6$ (72.6 mg, 0.04 mmol) and $[Cu(MeCN)_4]PF_6$ (7.45 mg, 0.02 mmol) in MeCN (10 mL); yield 72.8 mg (95%), m.p. 209 °C (decomp.); ^{13}C NMR (100 MHz, CD_3CN, 31 °C): $\delta = 65.9$, 69.0, 70.7, 71.1, 71.5, 71.7, 71.9, 72.2, 72.6 (CH_2), 105.5, 106.9, 111.2, 114.7, 114.9, 125.6, 126.3, 126.6, 126.9, 127.4, 131.8, 145.1, 145.5, 145.7 (CH), 96.4, 125.0, 137.7, 143.5, 146.6, 152.8, 153.7, 154.2, 154.7 (Cq); MS (LSIMS): $m/z = 3693$ $[M - PF_6]^+$, 3549 $[M - 2PF_6]^+$, 3403 $[M - 3PF_6]^+$, 3258 $[M - 4PF_6]^+$; $C_{152}H_{156}CuF_{54}N_{12}O_{20}P_9$ (3839.2): calcd C 47.55, H 4.10, N 4.38; found 47.77, H 3.91, N 4.49.

X-ray crystallography: Table 6 summarizes the crystal data, data collection, and refinement parameters for the complexes $[Re(CO)_3(Cl)\mathbf{L_1}](PF_6)_4$, $[Ag(\mathbf{L_1})_2](PF_6)_9$, $[\{Ru(bpy)_2\}_2\mathbf{L_2}](PF_6)_8$, and for the [2]catenane $\mathbf{L_4}\cdot 4PF_6$. All four structures were solved by direct methods and were refined by full matrix least-squares based on F^2. In $[Re(CO)_3Cl\mathbf{L_1}](PF_6)_4$, $[Ag(\mathbf{L_1})_2](PF_6)_9$, and $\mathbf{L_4}\cdot 4PF_6$, the cationic complexes were ordered and were refined anisotropically. In $[\{Ru(bpy)_2\}_2\mathbf{L_2}](PF_6)_8$, however, the centrosymmetric complex was found to exhibit 50/50 disorder in the orientation of the two chelating bipyridyl ligands, giving rise to both Δ and Λ configurations at the unique ruthenium center; all of these half-occupancy atoms, together with the full-occupancy atoms of the ordered macrocyclic ligand and the ruthenium center, were refined anisotropically. In $[Ag(\mathbf{L_1})_2](PF_6)_9$ and $[Re(CO)_3Cl\mathbf{L_1}](PF_6)_4$, there was found to be a mixture of both full and partial occupancy PF_6^- anions, the major occupancy atoms of which were refined anisotropically, the minor occupancy atoms isotropically. In $\mathbf{L_4}\cdot 4PF_6$, the PF_6^- and Cl^- anions were ordered and refined anisotropically. In $[\{Ru(bpy)_2\}_2\mathbf{L_2}](PF_6)_8$, two of the PF_6^- anions were ordered and were refined anisotropically, another was found to be disordered over two partial occupancy sites (the major occupancy orientation of which was refined anisotropically), and the remaining anion was found to be ordered but of only half occupancy, and was refined isotropically. The included benzene solvent molecules in $[Ag(\mathbf{L_1})_2](PF_6)_9$ were ordered and refined anisotropically; the MeCN molecules were distributed over multiple partial-occupancy sites and were refined isotropically. In $[Re(CO)_3Cl\mathbf{L_1}](PF_6)_4$, the benzene molecules were ordered (with one molecule sited on a center of symmetry) while the $MeNO_2$ molecules were distributed over a mixture of full and partial occupancy sites; the benzene molecules and major occupancy atoms of the nitromethane molecules were refined anisotropically, the minor occupancy atoms isotropically. The included MeCN molecules of $\mathbf{L_4}\cdot 4PF_6$ were also distributed over both full- and partial-occupancy positions, the full-occupancy atoms being refined anisotropically and the partial-occupancy atoms isotropically. In $[\{Ru(bpy)_2\}_2\mathbf{L_2}](PF_6)_8$, the two acetone molecules were found to be distributed over a mixture of three full- and partial-occupancy sites, with only the major occupancy atoms being refined anisotropically. The hydrogen atoms of all the structures were placed in calculated positions, assigned isotropic thermal parameters, $U(H) = 1.2\,U_{eq}(C)$ [$U(H) = 1.5\,U_{eq}(C\text{–}Me)$], and allowed to ride on their parent atoms. Computations were performed with the SHELXTL PC program system.[34] Crystallographic data (excluding structure factors) for the structures reported in this paper have been deposited with the Cambridge Crystallographic Data Centre as supplementary publication no. CCDC-100691. Copies of the data can be obtained free of charge on application to CCDC, 12 Union Road, Cambridge CB2 1EZ, UK (Fax: (+44) 1223-336-033; e-mail: deposit@ccdc.cam.ac.uk).

Acknowledgments: This research was supported by the Engineering and Physical Sciences Research Council in the United Kingdom and by the University of Bologna (Funds for Selected Research Topics) and CNR (Progetto Strategico Tecnologie Chimiche Innovative) in Italy, and by the EU (TMR grant FMRX-CT96-0076).

Received: September 10, 1997 [F817]

[1] a) J. S. Lindsey, *New J. Chem.* **1991**, *15*, 153–180; b) G. M. Whitesides, J. P. Mathias, C. T. Seto, *Science* **1991**, *254*, 1312–1319; c) D. Philp, J. F. Stoddart, *Synlett* **1991**, 445–448; d) D. B. Amabilino, J. F. Stoddart, *New Scientist* 19 Feb. **1994**, No. 1913, pp. 25–29; e) J.-M. Lehn, *Supramolecular Chemistry*, VCH, Weinheim, **1995**; f) D. Philp, J. F. Stoddart, *Angew. Chem.* **1996**, *108*, 1242–1286; *Angew. Chem. Int. Ed. Engl.* **1996**, *35*, 1154–1196.

[2] a) J.-M. Lehn, A. Rigault, J. Siegel, J. Harrowfield, B. Chevrier, D. Moras, *Proc. Natl. Acad. Sci. USA* **1987**, *84*, 2565–2569; b) E. C.

Table 6. Crystal data, data collection, and refinement parameters.[a]

	$[Re(CO)_3Cl\mathbf{L_1}](PF_6)_4$	$[Ag(\mathbf{L_1})_2](PF_6)_9$	$[\{Ru(bpy)_2\}_2](PF_6)_7$	$\mathbf{L_4}\cdot 4PF_6$
Formula	$C_{43}H_{34}N_6O_3ClRe\cdot 4PF_6$	$C_{80}H_{68}N_{12}Ag\cdot 9PF_6$	$C_{84}H_{68}N_{16}Ru_2\cdot 7PF_6$	$C_{76}H_{78}N_6O_{10}\cdot 2PF_6\cdot 2Cl$
Solvent	$5MeNO_2\cdot 1.5PhH$	$4PhH\cdot 4MeCN$	$4Me_2CO$	6MeCN
Formula weight	1906.7	3086.7	2750.8	1842.6
Color, habit	yellow/orange prisms	pale yellow needles	orange/red plates	red prisms
Crystal size (mm)	$0.33\times 0.27\times 0.27$	$0.67\times 0.30\times 0.18$	$0.80\times 0.77\times 0.10$	$0.30\times 0.30\times 0.17$
Lattice type	monoclinic	monoclinic	triclinic	triclinic
Space group	$P2_1/c$, 14	$C2/c$, 15	$P\bar{1}$, 2	$P\bar{1}$, 2
T (K)	293	198	203	173
a (Å)	13.415(1)	45.182(3)	13.465(2)	11.951(1)
b (Å)	22.407(2)	15.942(2)	13.776(2)	15.165(1)
c (Å)	26.524(3)	18.252(3)	22.115(4)	26.185(2)
α (°)	–		88.05(1)	97.48(1)
β (°)	103.32(1)	98.11(1)	73.61(1)	90.57(1)
γ (°)	–	–	68.33(1)	106.12(1)
V (Å^3)	7758(1)	13015(3)	3646(1)	4514.8(5)
Z	4	4[b]	1[c]	2
ρ_{calcd} (g cm^{-3})	1.632	1.575	1.253	1.355
$F(000)$	3796	6224	1383	1920
Radiation	$Cu_{K\alpha}$	$Cu_{K\alpha}$[d]	$Cu_{K\alpha}$[d]	$Cu_{K\alpha}$[d]
μ (mm^{-1})	5.26	3.47	3.29	1.74
θ range	2.6–55.0	2.0–60.0	3.7–55.0	1.7– 57.0
No. of unique reflns measured	9746	9624	8391	12147
No. of unique reflns observed, $\lvert F_o\rvert > 4\sigma(\lvert F_o\rvert)$	6649	7428	5031	7963
Absorption correction	semiempirical	semiempirical	empirical	–
Maximum, minimum transmission	0.23, 0.13	0.60, 0.29	0.84, 0.45	–
No. of variables	1073	896	998	1133
R_1[e]	0.059	0.093	0.124	0.088
wR_2[f]	0.154	0.256	0.346	0.212
Weighting factors a, b[g]	0.084, 10.668	0.185, 39.944	0.298, 2.770	0.133, 6.440
Largest difference peak, hole (e Å^{-3})	0.76, −0.37	0.83, −1.04	1.82, −0.53	0.62, −0.45

[a] Details in common: graphite-monochromated radiation, ω-scans, Siemens P4 diffractometer, refinement based on F^2. [b] The molecule has crystallographic C_2 symmetry. [c] The molecule has crystallographic C_i symmetry. [d] Rotating anode source. [e] $R_1 = \Sigma\,||F_o| - |F_c||/\Sigma\,|F_o|$. [f] $wR_2 = \sqrt{\{\Sigma[w(F_o^2 - F_c^2)^2]/\Sigma[w(F_o^2)^2]\}}$. [g] $w^{-1} = \sigma^2(F_o^2) + (aP)^2 + bP$.

Constable, *Tetrahedron* **1992**, *48*, 10013 – 10059; c) R. Krämer, J.-M. Lehn, A. De Cian, J. Fischer, *Angew. Chem.* **1993**, *105*, 764 – 767; *Angew. Chem. Int. Ed. Engl.* **1993**, *32*, 703 – 706; d) E. C. Constable, E. R. Heirtzler, M. Neuburger, M. Zhender, *Supramol. Chem.* **1995**, *5*, 197 – 200; e) C. R. Woods, M. Benaglia, F. Cozzi, J. S. Siegel, *Angew. Chem.* **1996**, *108*, 1937 – 1939; *Angew. Chem. Int. Ed. Engl.* **1996**, *35*, 1830 – 1833; f) A. F. Williams, *Chem. Eur. J.* **1997**, *3*, 15 – 19.

[3] a) C. O. Dietrich-Buchecker, J.-P. Sauvage, *Bioorganic Chemistry Frontiers*, *Vol. 2*, Springer, Berlin, **1991**, 197 – 248; b) J.-P. Sauvage, *Acc. Chem. Res.* **1990**, *23*, 319 – 327; c) D. Cardenas, A. Livoreil, J.-P. Sauvage, *J. Am. Chem. Soc.* **1996**, *118*, 11980 – 11981.

[4] a) C. O. Dietrich-Buchecker, J.-P. Sauvage, *Angew. Chem.* **1989**, *101*, 192 – 194; *Angew. Chem. Int. Ed. Engl.* **1989**, *28*, 189 – 192; b) C. O. Dietrich-Buchecker, J.-P. Sauvage, A. De Cian, J. Fischer, *J. Chem. Soc. Chem. Commun.* **1994**, *28*, 2231 – 2233; c) C. O. Dietrich-Buchecker, J.-P. Sauvage, N. Armaroli, P. Ceroni, V. Balzani, *Angew. Chem.* **1996**, *108*, 1190 – 1193; *Angew. Chem. Int. Ed. Engl.* **1996**, *35*, 1119 – 1121.

[5] a) F. Moulines, L. Djakovitch, R. Boese, B. Gloaguen, W. Thiel, J.-L. Fillaut, M.-H. Delville, D. Astruc, *Angew. Chem.* **1993**, *105*, 1132 – 1134; *Angew. Chem. Int. Ed. Engl.* **1993**, *32*, 1075 – 1077; b) S. Serroni, S. Campagna, A. Juris, M. Venturi, V. Balzani, G. Denti, *Gazz. Chim. Ital.* **1994**, *124*, 423 – 427; c) S. Campagna, G. Denti, S. Serroni, A. Juris, M. Venturi, V. Ricevuto, V. Balzani, *Chem. Eur. J.* **1995**, *1*, 211 – 221; d) G. Denti, S. Campagna, V. Balzani in *Mesomolecules: from Molecules to Materials* (Eds.: D. Mendenhall, A. Greensberg, J. Liebman), Chapman and Hall, New York, **1995**, pp. 69 – 106; e) Y.-H. Liao, J. R. Moss, *Organometallics* **1995**, *14*, 2130 – 2132; f) G. R. Newkome, R. Guther, C. N. Moorefield, F. Cardullo, L. Echegoyen, E. Perez-Cordero, H. Luftmann, *Angew. Chem.* **1995**, *107*, 2159 – 2162; *Angew. Chem. Int. Ed. Engl.* **1995**, *34*, 2023 – 2026; g) W. T. S. Huck, F. C. J. M. van Veggel, B. L. Kropman, D. H. A. Blank, E. G. Kein, M. M. A. Smithers, D. N. Reinhoudt, *J. Am. Chem. Soc.* **1995**, *117*, 8293 – 8294; h) D. Armspach, M. Cattalini, E. C. Constable, C. E. Housecroft, D. Phillips, *Chem. Commun.* **1996**, *15*, 1823 – 1824; i) S. Achar, J. J. Vittal, R. J. Puddephatt, *Organometallics* **1996**, *15*, 43 – 50; j) J. Issberner, F. Vögtle, L. De Cola, V. Balzani, *Chem. Eur. J.* **1997**, *3*, 706 – 712.

[6] a) V. Balzani, F. Scandola, *Supramolecular Photochemistry*, Ellis Horwood, Chichester (UK), **1991**; b) A. P. de Silva, C. P. McCoy, *Chem. Ind.* **1994**, 992 – 996; c) V. Balzani, A. Credi, F. Scandola, *Chim. Ind. (Rome)* **1996**, *78*, 1221 – 1231; d) P. R. Ashton, R. Ballardini, V. Balzani, S. E. Boyd, A. Credi, M. T. Gandolfi, M. Gómez-López, S. Iqbal, D. Philp, J. A. Preece, L. Prodi, H. G. Ricketts, J. F. Stoddart, M. S. Tolley, M. Venturi, A. J. P. White, D. J. Williams, *Chem. Eur. J.* **1997**, *3*, 152 – 170.

[7] V. Balzani, A. Juris, M. Venturi, S. Campagna, S. Serroni, *Chem. Rev.* **1996**, *96*, 759 – 833.

[8] A. Juris, V. Balzani, F. Barigelletti, S. Campagna, P. Belser, A. von Zelewsky, *Coord. Chem. Rev.* **1988**, *84*, 85 – 277.

[9] T. J. Meyer, *Acc. Chem. Res.* **1989**, *22*, 163 – 170.

[10] F. Scandola, M. T. Indelli, C. Chiorboli, C. A. Bignozzi, *Top. Curr. Chem.* **1990**, *158*, 73 – 149.

[11] K. Kalyanasundaram, *Photochemistry of Polypyridine and Porphyrin Complexes*, Academic Press, London, **1991**.

[12] D. B. Amabilino, J. F. Stoddart, *Chem. Rev.* **1995**, *95*, 2725 – 2828.

[13] M. Asakawa, P. R. Ashton, S. E. Boyd, C. L. Brown, S. Menzer, D. Pasini, J. F. Stoddart, M. S. Tolley, A. J. P. White, D. J. Williams, P. G. Wyatt, *Chem. Eur. J.* **1997**, 463 – 481.

[14] While this work was in progress, the compound $[Ru(bpy)_2\mathbf{L_3}](PF_6)_6$ was mentioned in the literature; see: A. C Benniston, A. Harriman, in *Physical Supramolecular Chemistry* (Eds.: L. Echegoyen, A. E. Kaifer), NATO ASI Series, Kluwer Academic, Dordrecht (the Netherlands), **1996**, pp. 179 – 197—and subsequently its synthesis

0947-6539/98/0404-0606 $ 17.50+.50/0 *Chem. Eur. J.* **1998**, *4*, No. 4

was described, as well: A. C. Benniston, P. R. Mackie, A. Harriman, *Tetrahedron Lett*. **1997**, *38*, 3577–3580; finally, a communication dealing with photoinduced electron transfer processes in the compounds $[Ru(bpy)_2\mathbf{L}_1]^{6+}$ and $[Ru(bpy)_2\mathbf{L}_3]^{6+}$ has also appeared recently; see: A. C. Benniston, P. R. Mackie, A. Harriman, *Angew. Chem.* **1998**, *110*, 376–378; *Angew. Chem. Int. Ed.* **1998**, *37*, 354–356.

[15] S. Gould, G. F. Strouse, T. J. Meyer, B. P. Sullivan, *Inorg. Chem*. **1991**, *30*, 2942–2949.

[16] O. Kocian, R. J. Mortimer, P. D. Beer, *Tetrahedron Lett.* **1990**, *31*, 5069–5072.

[17] L. D. Ciana, W. J. Dressick, A. von Zelewsky, *J. Heterocycl. Chem*. **1990**, *27*, 163–165.

[18] P. L. Anelli, P. R. Ashton, R. Ballardini, V. Balzani, M. Delgado, M. T. Gandolfi, T. T. Goodnow, A. E. Kaifer, D. Philp, M. Pietraszkiewicz, L. Prodi, M. V. Reddington, A. M. Z. Slawin, N. Spencer, J. F. Stoddart, C. Vicent, D. J. Williams, *J. Am. Chem. Soc.* **1992**, *114*, 193–218.

[19] D. B. Amabilino, P. R. Ashton, L. Pérez-García, J. F. Stoddart, *Angew. Chem.* **1995**, *107*, 2569–2572; *Angew. Chem. Int. Ed. Engl.* **1995**, *34*, 2378–2380.

[20] The kinetic and thermodynamic data were calculated using two procedures: a) the *coalescence method*, where values for the rate constant k_c at the coalescence temperature (T_c) were calculated (I. O. Sutherland, *Annu. Rep. NMR Spectrosc.* **1971**, *4*, 71–235) from the approximate expression $k_c = \pi(\Delta\tilde{\nu})/(2)^{1/2}$, where $\Delta\tilde{\nu}$ is the limiting chemical shift difference (Hz) between the coalescing signals in the absence of exchange; b) the *exchange method*, where values of k_{ex} were calculated (J. Sandström, *Dynamic NMR Spectroscopy*, Academic Press, London, **1982**; Ch. 6) from the approximate expression $k_{ex} = \pi(\Delta\tilde{\nu})$, where $\Delta\tilde{\nu}$ is the difference (Hz) between the line width at a temperature T_{ex}, where exchange of sites occurs, and the line width in the absence of exchange. The Eyring equation was subsequently employed to calculate $\Delta G_c^{\neq}$ or $\Delta G_{ex}^{\neq}$ values at T_c or T_{ex}, respectively.

[21] M. S. Henry, M. Z. Hoffman, *J. Phys. Chem.* **1979**, *83*, 618–625; A. B. P. Lever, *Inorganic Electronic Spectroscopy*, Elsevier, Amsterdam, **1984**, Ch. 5, p. 296.

[22] The absence of an eighth counterion in the final difference electron density map forces us to conclude that the structure contains a mixture of Ru^{I} and Ru^{II} oxidation states.

[23] This disorder is not a consequence of the choice of $P\bar{1}$ as the space group. Attemps to resolve the structure into molecules of one chirality only and refining them in $P1$ still produced 50:50 superimposed images of both chiralities.

[24] P. R. Ashton, R. Ballardini, V. Balzani, A. Credi, M. T. Gandolfi, D. J. F. Marquis, S. Menzer, L. Pérez-Garcia, L. Prodi, J. F. Stoddart, M. Venturi, A. J. P. White, D. J. Williams, *J. Am. Chem. Soc.* **1995**, *117*, 11171–11197.

[25] a) M. Wrighton, D. L. Morse, *J. Am. Chem. Soc.* **1974**, *96*, 998–1003; b) K. Kalyanasundaram, *J. Chem. Soc. Faraday Trans. 2* **1986**, *82*, 2401–2415.

[26] G. L. Gaines, III, M. P. O'Neil, W. A. Svec, M. P. Niemczyk, M. R. Wasielewski, *J. Am. Chem. Soc.* **1991**, *113*, 719–721; b) P. Chen, T. J. Meyer, *Inorg. Chem.* **1996**, *35*, 5520–5524.

[27] S. Roffia, M. Marcaccio, C. Paradisi, F. Paolucci, V. Balzani, S. Serroni, S. Campagna, G. Denti, *Inorg. Chem.* **1993**, *32*, 3003–3009.

[28] Upon oxidation, the catenane $\mathbf{2}^{4+}$ shows two not fully reversible processes at $+1.30$ V and $+1.55$ V, which can be attributed to the alongside and inside 1/5DMN units of the crown ether, respectively.

[29] D. D. Perrin, W. F. L. Armarego, *Purification of Laboratory Chemicals*, Pergamon, Oxford, **1989**.

[30] P. R. Ashton, E. J. T. Chrystal, J. P. Mathias, K. P. Parry, A. M. Z. Slawin, N. Spencer, J. F. Stoddart, D. J. Williams, *Tetrahedron Lett*. **1987**, *28*, 6367–6370.

[31] C. L. Brown, D. Philp, N. Spencer, J. F. Stoddart, *Israel J. Chem.* **1992**, *32*, 61–67.

[32] G. J. Kubas, *Inorg. Synthesis* **1971**, *19*, 90–92.

[33] A. Launikonis, P. A. Lay, A. W.-H. Mau, A. M. Sargeson, W. H. F. Sasse, *Aust. J. Chem*. **1986**, *39*, 1053–1062.

[34] SHELXTL PC version 5.03, Siemens Analytical X-Ray Instruments, Madison, WI, **1994**.